Bam complex associated proteins in *Escherichia coli* are functionally linked to peptidoglycan biosynthesis, membrane fluidity and DNA replication

Jack A. Bryant[1,2*†], Kara A. Staunton[1†], Hannah M. Doherty[1], Micheal B. Alao[1], Xuyu Ma[1], Joanna Morcinek-Orłowska[3], Emily C. A. Goodall[4], Jessica Gray[4], Mathew Milner[1,5,6], Jeffrey A. Cole[1], Felicity de Cogan[7], Timothy J. Knowles[1], Monika Glinkowska[3], Danesh Moradigaravand[5,6*], Ian R. Henderson[4*], Manuel Banzhaf[1,8*].

† These authors contributed equally.

* Correspondence should be addressed to Jack A. Bryant – j.a.bryant@bham.ac.uk, Manuel Banzhaf – m.banzhaf@bham.ac.uk, Danesh Moradigaravand - danesh.moradigaravand@kaust.edu.sa, or Ian R. Henderson - i.henderson@imb.uq.edu.au

[1]Institute of Microbiology and Infection, School of Biosciences, University of Birmingham, Edgbaston, B15 2TT, United Kingdom,

[2]School of Life Sciences, University of Nottingham, Nottingham, NG7 2RD, United Kingdom,

[3]Department of Biology, University of Gdańsk, 80-308 Gdańsk, Poland,

[4]Institute for Molecular Bioscience, University of Queensland, St. Lucia, 4072, Australia.

[5]Laboratory for Infectious Disease Epidemiology, KAUST Smart-Health Initiative and Biological and Environmental Science and Engineering Division, King Abdullah University of Science and Technology, Thuwal, Makkah 23955-6900, Saudi Arabia

[6]KAUST Computational Bioscience Research Center, King Abdullah University of Science and Technology, Thuwal, Makkah 23955-6900, Saudi Arabia

[7]School of Pharmacy, University of Nottingham, Nottingham, NG7 2RD, United Kingdom,

[8]Newcastle University Biosciences Institute, Faculty of Medical Sciences, Newcastle University, Newcastle upon Tyne, NE2 4HH, UK.

Abstract

Biogenesis of the bacterial outer membrane is key to survival and antibiotic resistance. Central to this is the β-barrel assembly machine (Bam) complex and its associated chaperones, which are responsible for outer membrane protein (OMP) transport and insertion. The *Escherichia coli* Bam complex consists of two essential subunits, BamA and BamD, and three non-essential lipoproteins, BamB, BamC and BamE. Optimal Bam function is further dependent on the non-essential chaperones DegP, Skp and SurA. Despite intensive study, the specific function of these non-essential Bam-associated proteins remains unknown. Here, we analysed knockout strains for each gene by phenotypic screening, conservation analysis and high-throughput genetics. We reveal that Bam activity is affected by outer membrane lipid composition and that enterobacterial common antigen is essential in the absence of the chaperone SurA. We also show that components of peptidoglycan are conditionally essential with Bam accessory lipoproteins and that DNA replication is perturbed in the absence of BamB. Together, our data indicates potential mechanisms for coordination of OMP biogenesis with processes such as LPS and peptidoglycan biogenesis, and DNA replication.

Keywords:

Bam complex / TraDIS / Escherichia coli / DNA replication / peptidoglycan synthesis

45 **Introduction**

46 The Gram-negative outer membrane is instrumental for virulence, antimicrobial resistance,
47 and immune evasion. The outer membrane is an asymmetric lipid bilayer consisting of
48 phospholipid on the inner leaflet, lipopolysaccharide (LPS) on the outer leaflet, integral outer
49 membrane proteins (OMPs) and associated lipoproteins. Biogenesis of the outer membrane
50 is completed by several multi-component proteinaceous machines. Central to this is the β-
51 barrel assembly machine (Bam) complex, the essential protein machinery responsible for
52 folding and insertion of OMPs into the outer membrane, which then act as transporters, porins,
53 receptors, virulence factors, adhesins and enzymes (Konovalova et al., 2017, Rollauer et al.,
54 2015). All OMPs are synthesised in the cytoplasm before being trafficked through the inner
55 membrane to the periplasmic space by the Sec machinery. OMPs are prone to aggregation
56 and must be maintained in an unfolded state during their translocation to the Bam complex
57 (Ruiz et al., 2006). Three quality control proteins that chaperone OMPs across the periplasm
58 are SurA, Skp and DegP. The double mutants Δ*surA*Δ*skp* and Δ*surA*Δ*degP* are not viable,
59 which suggests that Skp, SurA and DegP might be functionally redundant (Rizzitello et al.,
60 2001). Indeed, the primary chaperone pathway to the Bam complex is thought to be SurA,
61 while Skp and DegP are suggested to form a secondary pathway that is amplified in stress
62 conditions (Sklar et al., 2007). However, single molecule studies with purified OmpC and Skp
63 or SurA demonstrate that the two proteins recognise different conformations of the OMP and
64 that while Skp is capable of dispersing aggregated OmpC, SurA is not. This suggests that Skp
65 and SurA have specialised roles in maintaining OMPs in a folding competent state during
66 periplasmic transit (Li et al., 2018).

67 Following transport across the periplasmic space, OMPs are received at the outer membrane
68 by the Bam complex. In *Escherichia coli*, the Bam complex is composed of two essential
69 subunits, the outer membrane β-barrel BamA and the lipoprotein BamD, and three non-
70 essential accessory lipoproteins, BamB, BamC and BamE (Hagan et al., 2010, Wu et al.,
71 2005). BamA is the central component of the complex and consists of a 16-stranded β-barrel

72 and five periplasmically localised POlypeptide-TRansport-Associated (POTRA) domains that
73 function to dock the accessory subunits (Gentle et al., 2005, Sánchez-Pulido et al., 2003). The
74 POTRA domains are hypothesised to interact with incoming unfolded OMP substrates and
75 feed them into the assembly machinery (Knowles et al., 2008). BamD is a lipoprotein
76 composed of five tetratricopeptide repeat (TPR) domains that interact with POTRA 5 of BamA
77 (Dong et al., 2012, Sandoval et al., 2011, Wu et al., 2005). The remaining components of the
78 complex are the accessory lipoproteins, BamB, BamC and BamE, which interact with BamA
79 and BamD to form a functionally coordinated ring structure under the BamA barrel on the
80 periplasmic face of the outer membrane (Bakelar et al., 2016, Browning et al., 2015, Gu et al.,
81 2016, Iadanza et al., 2016, Knowles et al., 2011).
82 The Bam complex accessory lipoproteins each contribute to full activity of the complex through
83 a shared redundant function of coordinating efficient BamA/D interaction in OMP engagement
84 and folding. Beyond this shared function, there is some limited information about specific roles
85 of these proteins in the cell (Hagan et al., 2010, Hart & Silhavy, 2020). For example, as part
86 of the Rcs stress response signalling pathway, the outer membrane lipoprotein RcsF is
87 threaded through an OMP during folding by the Bam complex and this process specifically
88 requires BamE (Konovalova et al., 2016). In addition, lethal jamming of the Bam complex in
89 the absence of BamE can be prevented by BamB (Hart et al., 2019, Tata & Konovalova, 2019).
90 BamB has also been shown to be important in folding of high-flux substrates (Charlson et al.,
91 2006). However, further information about the specific roles of BamB, BamC and BamE are
92 lacking (Hart & Silhavy, 2020).
93 In this study, we provide evidence for specialised function and show that changes to LPS
94 structure lead to increased membrane fluidity and decreased Bam complex activity. We also
95 identify that the cyclic form of enterobacterial common antigen (ECA), a periplasmic
96 carbohydrate, is essential in the absence of the chaperone protein SurA. Further to this we
97 demonstrate that the Bam accessory lipoproteins, including BamC, are essential in the
98 absence of the peptidoglycan stem-peptide component *meso*-DAP, providing a strong
99 phenotype for this poorly understood protein. Lastly, we show that loss of BamB causes the

100 cells to over-initiate DNA replication, which also becomes asynchronous, indicating potential
101 coordination between OMP biogenesis and DNA replication. Together, our data indicate
102 specialised roles for the Bam-associated proteins and highlights potential mechanisms for
103 coordination of OMP biogenesis with processes such as outer membrane lipid biogenesis,
104 peptidoglycan synthesis and DNA replication control.

105 **Results**

106 **Loss of Bam-associated proteins leads to distinct phenotypes**

107 We hypothesised that if the Bam-associated proteins have specialised roles in the cell it would
108 be unlikely that they phenocopy each other. Therefore, we tested fitness of Δ*bamB*, Δ*bamC*,
109 Δ*bamE*, Δ*surA*, Δ*skp* and Δ*degP* mutants of *E. coli* K-12 BW25113 compared to the parent
110 strain under various stresses. We arrayed the strains in 384-well format on solid agar plates
111 containing each stress or compound. Endpoint pictures were taken to quantify colony fitness
112 based on size by the image analysis software Iris (Kritikos et al., 2017). Fitness was scored
113 using the chemical genomics analysis software ChemGAPP Small by comparing the mean
114 colony size for the mutant in each condition to the mean colony size of that mutant in the LB
115 agar condition, which was normalised to a fitness score of 1 (Doherty et al., 2023). Fitness
116 scores below 1 represent decreased fitness, as a function of colony size compared to growth
117 on LB agar, and scores above 1 indicate increased fitness in that condition.

118 The fitness of each mutant across all conditions identified that the Δ*bamB* and Δ*surA* mutants
119 have the strongest fitness defects **(Fig 1)**. Correlation between each mutant fitness profile pair
120 was assessed by calculating the Pearson correlation coefficient. This demonstrated that
121 Δ*bamB* and Δ*surA* have a similar phenotypic profile with a correlation coefficient of 0.74, the
122 highest of all pairs of mutants **(Fig S1)**. Similar decreased fitness scores were observed for
123 both strains in the presence of bacitracin, carbenicillin, erythromycin, sodium dodecyl-sulfate
124 (SDS), osmotic stress conditions due to varied salt concentrations, and vancomycin **(Fig 1)**.
125 This is unsurprising as SurA is the major chaperone pathway for OMPs to reach the Bam
126 complex resulting in low fitness of Δ*bamB* and Δ*surA* when growing on LB at 37°C. However,
127 despite this functional link, they do not always phenocopy each other. For example, the Δ*bamB*
128 strain grew better in the presence of the MreB inhibitor A22 with a fitness score of 1.59, but
129 the Δ*surA* mutant was less fit in this condition (score of 0.51). The same was true in the
130 presence of doxycycline (Δ*bamB* – 1.65, Δ*surA* – 0.94) and hydroxyurea (Δ*bamB* – 0.68,
131 Δ*surA* – 1.14) **(Fig 1)**.

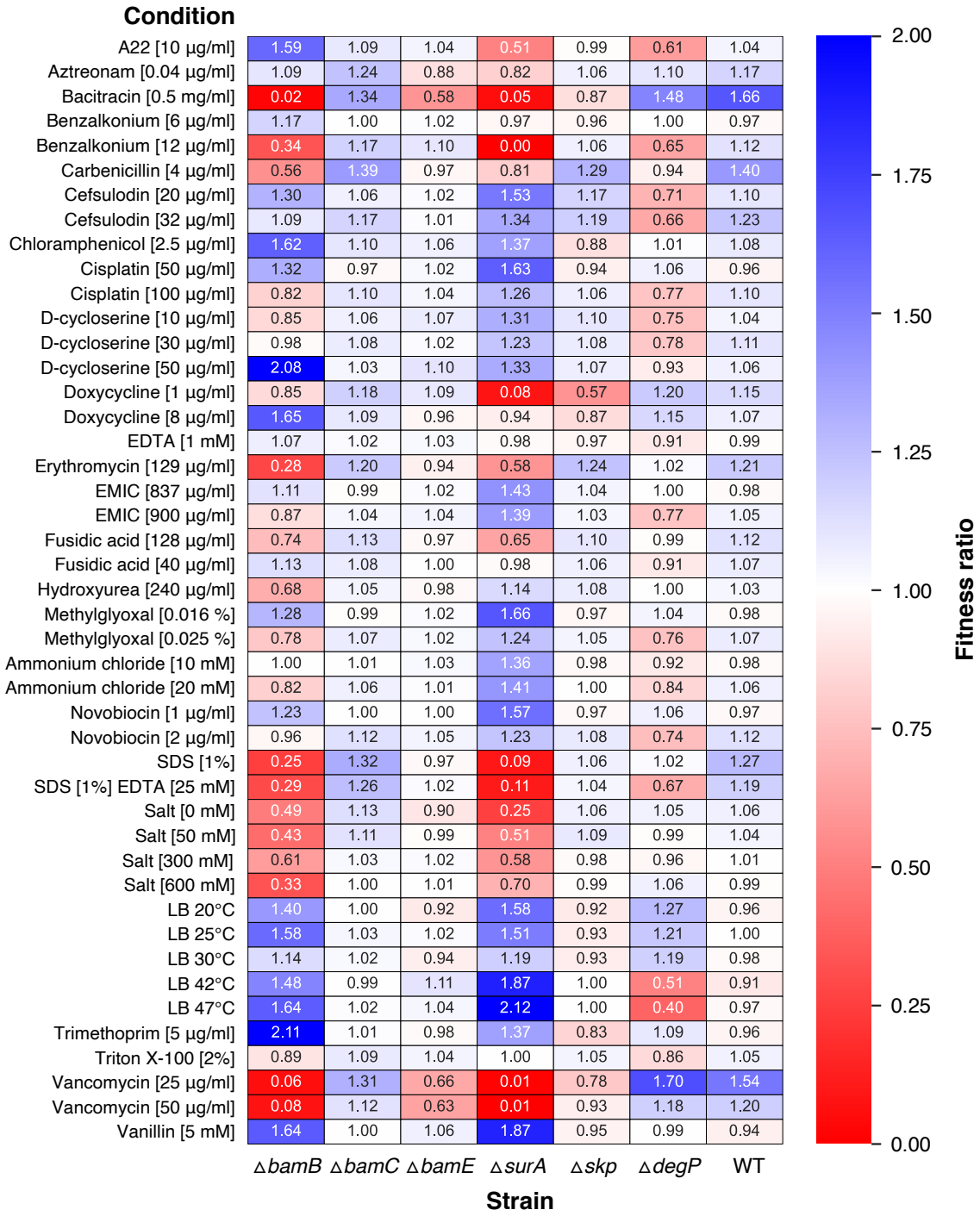

Figure 1 – Phenotypic profiling of mutants lacking Bam-associated proteins
Heat map of fitness scores for the *E. coli* BW25113 parent strain and Δ*bamB*, Δ*bamC*, Δ*bamE,* Δ*surA*, Δ*skp*, or Δ*degP* mutants grown in various stress conditions. Colony size measurements for each condition were normalised by comparing to colony size of that strain when grown on LB medium at 37°C. Growth of each strain on LB is set to 1 and each condition normalised to this. Fitness scores above 1 represent better growth than the LB condition as measured by colony size and scores below 1 indicate smaller colony size than the LB condition. Some conditions are abbreviated due to space restrictions: EMIC - 1-Ethyl-3-methylimidazolium chloride, EDTA - Ethylenediaminetetraacetic acid, SDS – Sodium dodecyl sulfate.

144 The Δ*bamE* mutant only mildly correlated to Δ*bamB* with a coefficient of 0.51 **(Fig S1)**.
145 However, as expected both mutants were sensitive to vancomycin (Δ*bamB* – 0.06, Δ*bamE* –
146 0.66) and bacitracin (Δ*bamB* – 0.02, Δ*bamE* – 0.58) two antibiotics that exceed the exclusion
147 limit of outer membrane porins and to which sensitivity indicates damage to the permeability
148 barrier. In contrast, Δ*bamC* has no strong phenotypes and correlated most strongly with the
149 WT parent strain **(Fig 1 and Fig S1**). Similarly, to Δ*bamC*, the Δ*skp* mutant also has no strong
150 phenotypes in our screen. Surprisingly, Δ*degP* was negatively correlated with the other
151 periplasmic chaperone pathway group mutants Δ*skp* (-0.51) and Δ*surA* (-0.37) and with
152 Δ*bamE* (-0.68) due to opposing fitness scores in a range of stresses **(Fig. 1 and Fig S1)**.
153 Together, the phenotypic profiling data indicate that while there are shared phenotypes
154 between each knockout, we observe a broad range of unique, mutant specific phenotypes that
155 suggests specialised roles.
156
157 **TraDIS identifies unique synthetic lethal interactions for Bam-associated proteins.**
158 Considering that the Bam-associated proteins have specialised function, we sought to find
159 their genetic interaction networks by using Transposon-Directed Insertion site Sequencing
160 (TraDIS). When TraDIS libraries are generated in single gene deletion mutant backgrounds,
161 the insertion frequencies of genes/regions compared to wild-type cells identifies genes that
162 become more important for survival in the mutant backgrounds. These genes are termed
163 conditionally essential, and help to identify co-dependencies of processes that the candidate
164 gene might be involved in. The method can also identify mutants that are more fit in the given
165 genetic background or condition (Cain et al., 2020, Goodall et al., 2021, Langridge et al., 2009,
166 Winkle et al., 2021). Therefore, the parent strain (*E. coli* BW25113) and Δ*bamB,* Δ*bamC,*
167 Δ*bamE,* Δ*surA,* Δ*skp,* or Δ*degP* mutants were transformed with a mini Tn5-kanamycin
168 transposon and recovered on LB agar at 37°C. Transposon mutants were then pooled and
169 transposon insertion sites identified by DNA sequencing as described previously (Goodall et
170 al., 2021). The BioTraDIS pipeline was used for data analysis in order to classify genes as

171 either essential or non-essential. Essential genes were then compared to the parent BW25113
172 TraDIS library to identify genes that became essential in the knockout strains (conditionally
173 essential) **(Table S1)** (Barquist et al., 2016). For quality control, two independent replicates of
174 each transposon library were sequenced over several sequencing runs. Individual sequencing
175 runs had a high correlation coefficient of ≥0.93 between samples and generated >6 million
176 TraDIS reads and >500,000 unique insertion sites for each strain **(Fig S2 and S3)**. Transposon
177 insertion sites were evenly mapped throughout the genome, with the exception of an increased
178 density around the origin of replication as expected due to gene dosage **(Fig S4)** (Cooper &
179 Helmstetter, 1968).
180 These experiments are aimed to identify novel genetic interactions, but this unbiased
181 approach will also uncover known synthetic lethal gene pairs that are still useful for us to
182 benchmark our data against. Indeed, we confirmed known genetic interactions between *surA*
183 and *skp* (Rizzitello et al., 2001), *degP* and *surA* (Rizzitello et al., 2001), *bamB* and *degP*
184 (Charlson et al., 2006) and *bamE* and *bamB* (Hart et al., 2019) **(Fig S5)**. The Δ*bamB,* Δ*bamC*
185 and Δ*bamE* TraDIS libraries allowed identification of 93, 92 and 29 conditionally essential
186 genes, respectively **(Fig 2A and Table S1)**. This is particularly surprising as there are no
187 known roles or dependencies for *bamC* and we did not observe strong phenotypes for Δ*bamC*
188 in our phenotypic screen **(Fig 1)**. Unfortunately, 54 of the genes identified as conditionally
189 essential in the Δ*bamC* background are of unknown function, therefore providing no
190 hypotheses for the role of BamC **(Table S1)**.
191 Next, we compared the conditionally essential gene lists to probe if they are involved in similar
192 processes or contribute to the same function within the cell. In the case that all three Bam
193 accessory proteins solely contribute to Bam function, we would expect to find significant
194 overlap between mutants. However, we found a large number of unique conditionally essential
195 genes for each (62, 57 and 5 for Δ*bamB,* Δ*bamC* and Δ*bamE,* respectively), indicating
196 potential specialised roles in the cell **(Fig 2A)**.
197 For the OMP chaperone pathway mutants we identified 247, 87 and 35 conditionally essential
198 genes for the Δ*surA,* Δ*degP* and Δ*skp* mutants, respectively **(Fig 2A)**. As the Δ*surA* mutant

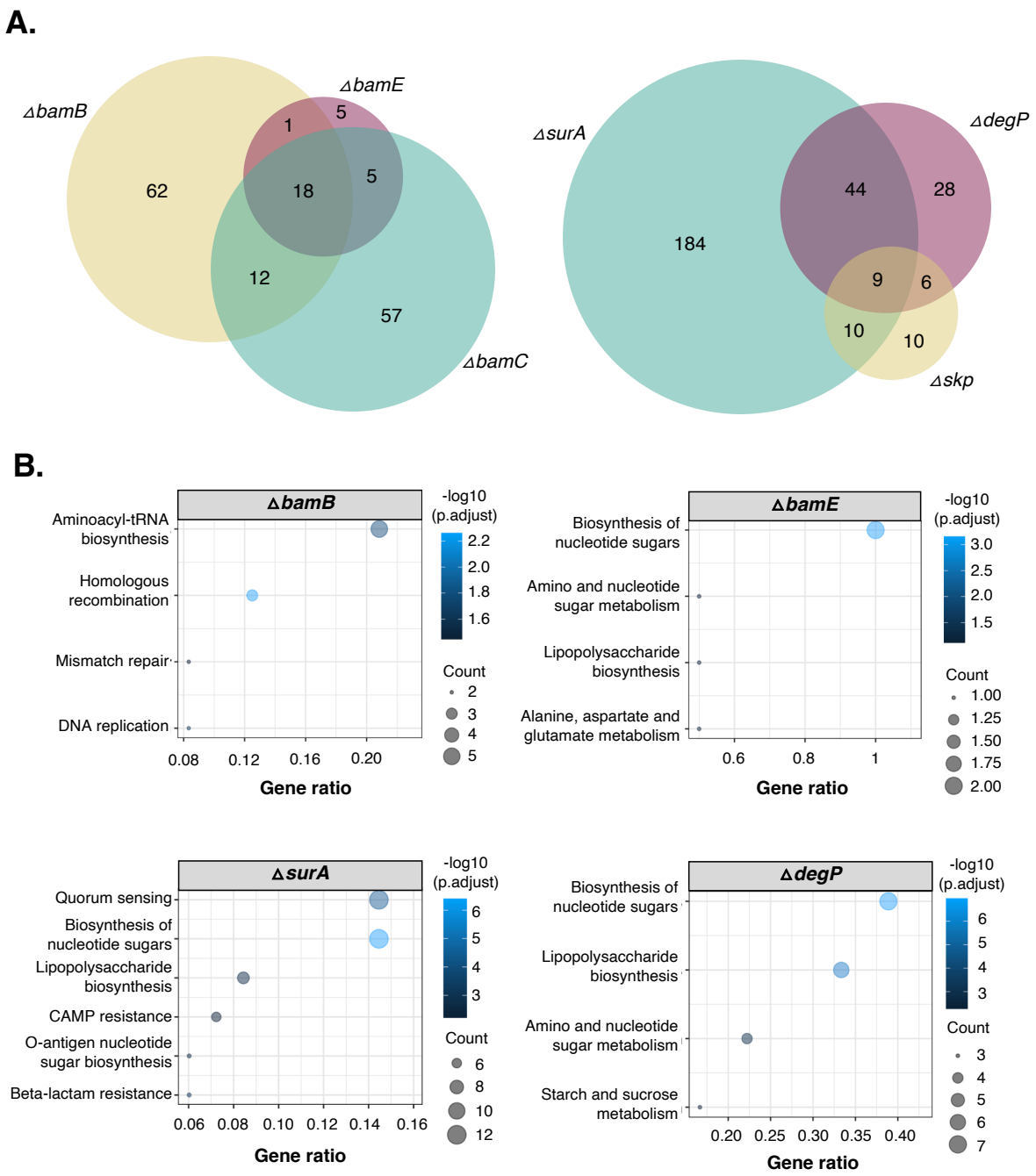

Figure 2 - Genetic interaction analysis of Bam-associated genes by TraDIS
TraDIS libraries were constructed in the *E. coli* BW25113 parent strain and Δ*bamB*, Δ*bamC*, Δ*bamE,* Δ*surA*, Δ*skp*, or Δ*degP* mutants in order to identify genes that become essential in each knockout strain compared to the parent library (conditionally essential). **A.** Venn diagrams showing conditionally essential genes identified within the Δ*bamB*, Δ*bamC* and Δ*bamE* TraDIS libraries or the Δ*surA*, Δ*skp* and Δ*degP* libraries. **B.** Analysis of KEGG categories enriched in conditionally essential gene lists in the Δ*bamB*, Δ*bamE,* Δ*surA* and Δ*degP* TraDIS libraries, represented as bubble plots. No data is shown for the Δ*bamC* and Δ*skp* conditionally essential gene lists as there was no significant enrichment of any KEGG categories.

212 had many strong phenotypes when probed against stresses **(Fig 1)**, this could potentially
213 explain the large number of conditionally essential genes compared to the other OMP
214 chaperone mutants **(Fig 2A)**. Of the 87 conditionally essential genes in the Δ*degP* dataset,
215 only 15 were also in the Δ*skp* background, despite DegP and Skp being assumed to be part
216 of the same arm of the chaperone pathway. These results suggest that while there is functional
217 redundancy between the SurA and DegP/Skp chaperone pathways, the function of the
218 chaperones under specific chemical and genetic conditions is likely specialised **(Fig 1 and**
219 **2A)**.
220 In order to determine the functions and associated pathways of the conditionally essential
221 genes identified in the mutant backgrounds, we completed GO and KEGG analyses.
222 Enrichment analysis of KEGG pathways for the Δ*bamC* and Δ*skp* datasets resulted in no
223 significant enrichment of any one category. However, genes involved in "Lipopolysaccharide
224 biosynthesis" and "Biosynthesis of nucleotide sugars" were enriched in the Δ*surA*, Δ*degP* and
225 Δ*bamE* conditionally essential gene lists and "O-antigen nucleotide sugar biosynthesis" was
226 enriched in the Δ*surA* background **(Fig 2B and Table S2)**. The most enriched KEGG pathway
227 in the Δ*bamB* dataset was "Aminoacyl-tRNA biosynthesis", however these genes all encode
228 tRNAs and are on average 75 bp in length. Visual inspection of these gene regions identified
229 sparse insertion density within the local genomic area leading to a likely false positive for
230 conditional essentiality. The Δ*bamB* dataset is also significantly enriched for three other KEGG
231 pathways: "Homologous recombination", "Mismatch repair" and "DNA replication" **(Fig 2B and**
232 **Table S2)**. Together, the KEGG pathway enrichment analysis identifies the importance of LPS
233 and ECA biosynthesis in these mutants as well as a potential link between OMP biogenesis
234 and DNA replication, which directed our further investigations.
235
236 **Genes required for heptose incorporation into LPS demonstrate synthetic lethality with**
237 ***bamB, surA* and *degP***
238 We identified that fewer mutants were recovered with transposon insertions in genes involved
239 in LPS assembly in the Δ*bamB*, Δ*surA* and Δ*degP* backgrounds than in the parent. In addition,

240 genes involved in “Biosynthesis of nucleotide sugars” were significantly enriched, with genes
241 identified being involved in the synthesis of heptose, a core component of LPS **(Fig 2B and**
242 **Table S2)**. Despite this category being enriched in the Δ*bamE* dataset, we found this was due
243 to one gene in particular and that the result was actually specific to the Δ*bamB*, Δ*surA* and
244 Δ*degP* TraDIS libraries **(Fig 3A and Fig S6)**. Synthesis of heptose consists of five main steps
245 before it is incorporated into the LPS inner core **(Fig 3B)**. In the Δ*surA* and the Δ*degP* TraDIS
246 libraries, all four genes involved in synthesis of heptose were essential: *gmhA*, *gmhB*, *hldE*
247 and *waaD*. In the Δ*bamB* background all were essential except for *gmhB,* which is potentially
248 because a Δ*gmhB* mutant is partially defective in LPS core synthesis, but is not completely
249 devoid of heptose (Kneidinger et al., 2002). These data suggest that heptose production was
250 functionally more important in Δ*degP* and Δ*surA* than in the Δ*bamB* mutant.
251 The incorporation of heptose into the LPS structure was also functionally important. In Δ*degP*
252 and Δ*surA* mutants, the genes *waaC* and *waaF* were conditionally essential, which are
253 responsible for transfer of the first and second heptose onto the LPS inner core, respectively
254 **(Fig 3A and 3B)** (Gronow et al., 2000, Kadrmas & Raetz, 1998). In contrast, in the Δ*bamB*
255 mutant, *waaC* was conditionally essential whereas *waaF* was not. This implies that while
256 Δ*degP* and Δ*surA* mutants are not able to tolerate having LPS with only one heptose residue,
257 the Δ*bamB* mutant is.
258

259 **LPS truncation leads to increased membrane fluidity and decreased Bam complex**
260 **activity**

261 Increased outer membrane fluidity decreases Bam activity and modifications to LPS structure
262 can lead to changes in membrane fluidity (Storek et al., 2019). Thus, we hypothesised that
263 changes in LPS core structure would affect membrane fluidity to differing degrees, which could
264 affect Bam complex efficiency. To test this hypothesis we assessed membrane fluidity and
265 Bam complex activity in strains lacking the genes encoding the heptose biosynthesis pathway
266 (Δ*gmhA*, Δ*gmhB,* Δ*hldE*, and Δ*waaD*) and LPS core synthesis (Δ*waaC*, Δ*waaF*, Δ*waaP*,
267 Δ*waaG* and Δ*waaY*) **(Fig 3)**. There were no differences in insertion index for the gene *waaY,*

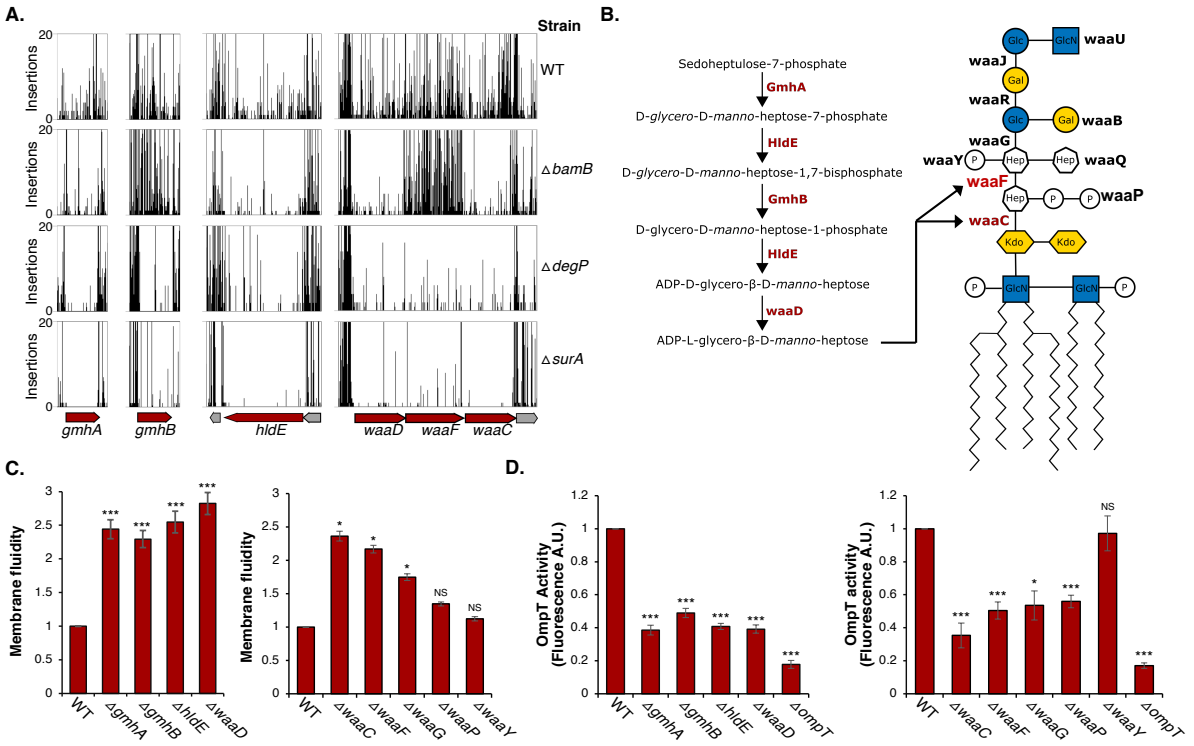

Figure 3 - Incorporation of heptose into LPS is essential in Δ*bamB,* Δ*surA* and Δ*degP*
A. Transposon insertions in the genes *gmhA*, *gmhB*, *hldE, waaD, waaC,* and *waaF* in the parent, Δ*bamB,* Δ*surA* and Δ*degP* TraDIS libraries. Transposon cut-off is set to 20. Essential genes are represented as red arrows. **B**. Schematic of the heptose biosynthesis pathway and LPS structure in *E. coli* K-12 BW25113 with gene labels for LPS biosynthesis enzymes indicated next to the linkage they form or component they ligate. Enzymes identified as conditionally-essential are labelled in red text. **C.** Membrane fluidity was measured in Δ*gmhA,* Δ*gmhB,* Δ*hldE,* Δ*waaD,* Δ*waaC*, Δ*waaF*, Δ*waaG*, Δ*waaP* and Δ*waaY* mutants and compared to the parent strain by using pyrenedeconoic acid fluorescence. **D.** To determine the extent of Bam complex activity, successful folding and insertion of OmpT into the outer membrane was measured in the Δ*gmhA,* Δ*gmhB,* Δ*hldE,* Δ*waaD,* Δ*waaC*, Δ*waaF*, Δ*waaG*, Δ*waaP*, Δ*waaY* and Δ*ompT* mutants and compared to the parent strain. For panels C and D, experiments were performed in biological and technical triplicate with standard deviation represented by error bars. Two sample t-tests were used to assess statistical significance of differences from the WT strain with *** indicating p-values of <0.001, * indicating p-values of <0.05, and NS as not significant (p-value ≥0.05).

285 which encodes the enzyme responsible for phosphorylation of the second heptose in the LPS
286 inner core. Therefore, Δ*waaY* should act as a control in this experiment (Yethon et al., 1998).
287 In addition, Δ*waaP* and Δ*waaG*, which are responsible for phosphate addition to the first
288 heptose, and incorporation of the first glucose, respectively (Parker et al., 1992), were included
289 as a small decrease in the insertion indexes for these genes were observed in the Δ*surA* and
290 Δ*degP* TraDIS datasets **(Fig S6).**
291 Fluidity of the membrane for each mutant was measured using the lipophilic pyrene probe,
292 pyrene decanoic acid. The pyrene monomer can undergo excimer formation and
293 demonstrates a shift in fluorescence, a process which is dependent on the ease of mobility
294 within the membrane (Kumar et al., 2002, Storek et al., 2018). Formation of the excimer was
295 measured and compared to that of the parent strain **(Fig 3C)**. The largest increase in
296 membrane fluidity occurred in knockouts of genes required for heptose biosynthesis: Δ*gmhA*,
297 Δ*gmhB,* Δ*hldE*, and Δ*waaD*. Of this group, the Δ*gmhB* mutant had the smallest increase in
298 membrane fluidity and this gene was also not essential in the Δ*bamB* background **(Fig 3A and**
299 **3C)**. Of the genes required for LPS core biosynthesis, membrane fluidity was higher in Δ*waaC*,
300 Δ*waaF* and Δ*waaG* than in the parent strain with the biggest change being in Δ*waaC* and the
301 smallest in Δ*waaG*. However, there was no significant increase in fluidity in the Δ*waaP* mutant.
302 Membrane fluidity of the Δ*waaF*, Δ*waaP* and Δ*waaG* mutants was intermediate between that
303 of the heptoseless Δ*waaC* mutant and the parent, with the severity of the effect correlating to
304 the severity of LPS core truncation. No significant change in membrane fluidity was measured
305 in the Δ*waaY* mutant control **(Fig 3C)**.
306 Next, we investigated whether impairment of heptose synthesis affected activity of the Bam
307 complex, which was monitored by an *in vivo* OmpT fluorescence assay. The outer membrane
308 protease OmpT is dependent on the Bam complex and is able to cleave a fluorogenic peptide,
309 which is monitored by increased fluorescence over time (Hagan et al., 2010). With the
310 exception of Δ*waaY*, all mutants demonstrated a minimum 40% decrease in OmpT activity
311 compared to the parent strain. The heptoseless Δ*waaC* mutant exhibited the greatest
312 decrease in OmpT activity. The effect of Δ*waaF*, Δ*waaP* and Δ*waaG* mutations on OmpT

313 activity levels was comparable to each other and intermediate between that of Δ*waaC* and the
314 parent strain **(Fig 3D)**. In summary, mutations that lead to heptoseless LPS had the biggest
315 increase in membrane fluidity and the lowest levels of OmpT activity with a graded response
316 based on the severity of LPS core truncations. This suggests there is a correlation between
317 LPS core structure, membrane fluidity and Bam complex activity that leads to a variety of Bam
318 complex activity levels depending on the form of LPS in the outer membrane.
319

320 **Generation of cyclic ECA is essential in the absence of the chaperone SurA**

321 Genes involved in 'Biosynthesis of nucleotide sugars' were significantly enriched as
322 conditionally essential in the Δ*surA* mutant. The genes identified are involved in biosynthesis
323 of ECA (**Fig 2B)**, which is a highly conserved carbohydrate-derived molecule present on the
324 external leaflet of the outer membrane and in the periplasm of Enterobacteriaceae (Kuhn et
325 al., 1988, Kunin, 1963). All of the ECA biosynthesis pathway genes were conditionally
326 essential with the exception of *wxyE,* which is required for survival of both the parent and the
327 Δ*surA* mutant **(Fig 4A and 4B)**. In addition, fewer mutants were recovered with transposon
328 insertions in the genes *rffH* and *rffG* than in the parent TraDIS library (**Fig 4A)**. The gene
329 products RffH and RffG catalyse the same enzymatic reaction and are homologous in
330 sequence to the genes RfbA and RfbB, respectively. However, they form part of different
331 operons and function in separate pathways despite *rffG* being able to complement an RfbB
332 defective strain (Marolda & Valvano, 1995, Sivaraman et al., 2002). This likely explains why
333 *rffH* and *rffG* are not entirely essential in the Δ*surA* background.
334 ECA exists in three forms that all share the same biosynthetic pathway: ECA that is covalently
335 linked to LPS (ECA_{LPS}), covalently linked to diacylglycerol-phosphate (ECA_{PG}), or a cyclic form
336 (ECA_{CYC}) (Kuhn et al., 1988, Rai & Mitchell, 2020). We sought to determine which form of ECA
337 is conditionally essential in Δ*surA*. Synthesis of ECA_{LPS} is facilitated by the O-antigen ligase
338 WaaL, which is responsible for attaching the ECA molecule onto the LPS core (Rai et al.,
339 2021, Schmidt et al., 1976). However, in the Δ*surA* TraDIS library, the gene *waaL* is non-
340 essential **(Fig 4C)**. This suggests that ECA_{LPS} is not essential in the Δ*surA* mutant.
341

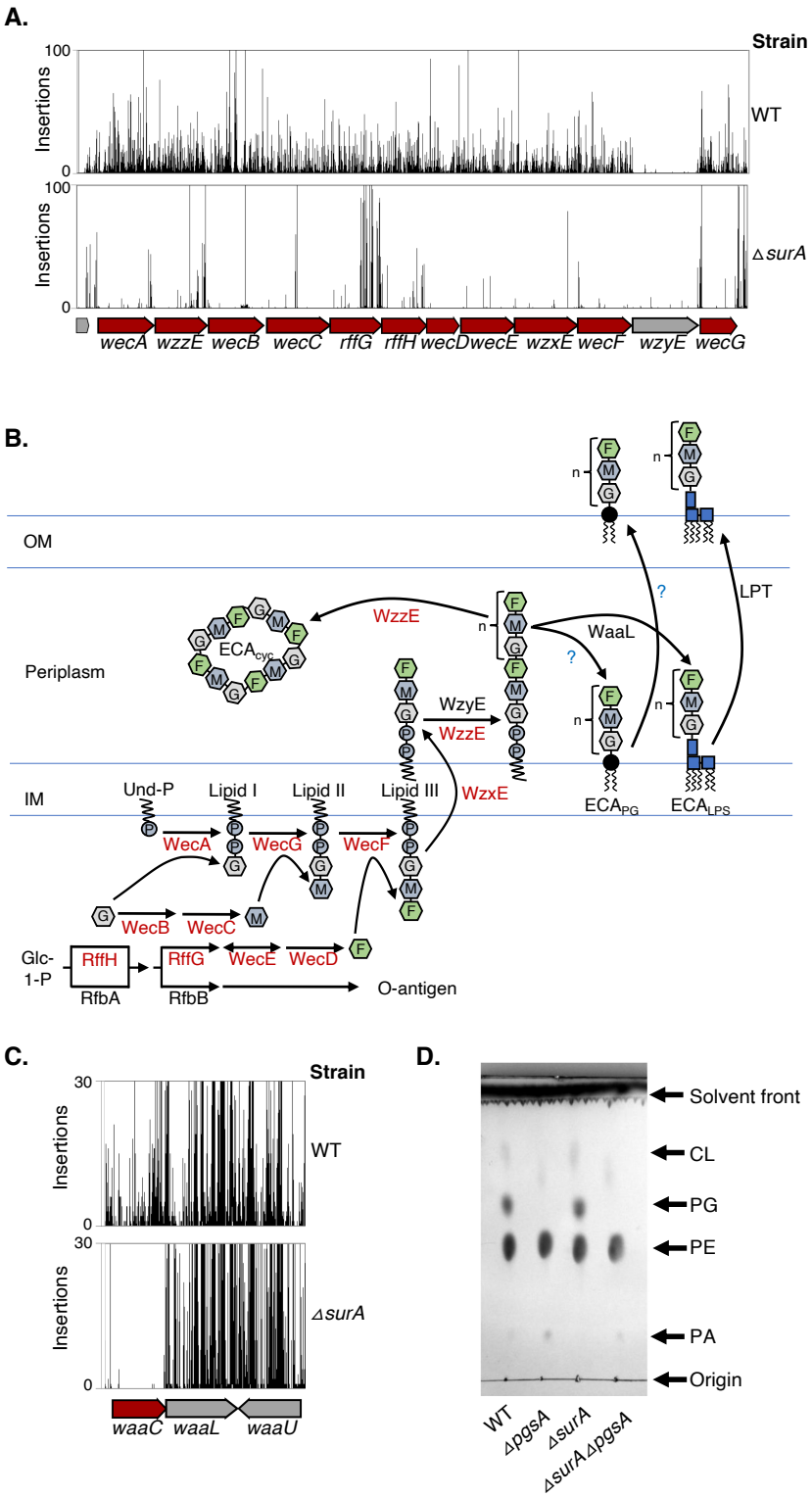

Figure 5 – Synthesis of ECA is essential in the absence of the chaperone SurA

A. Transposon insertions in genes of the ECA biosynthesis pathway in the parent or Δ*surA* mutant TraDIS libraries. Transposon cut-off is set to 100. Essential genes are represented as red arrows. **B.** Schematic representation of the ECA biosynthesis pathway with the names of proteins labelled next to the reaction for which they are responsible. Conditionally essential proteins are labelled in red text. **C.** Transposon insertions in the *waaL* gene in either the parent or Δ*surA* mutant TraDIS libraries. Transposon cut-off is set to 100. **D.** Analysis of phospholipid content in the parent or Δ*surA* mutant with further mutations to disrupt synthesis of the major anionic phospholipids. The Δ*pgsA* *and* Δ*surA*Δ*pgsA* strains are also Δ*lpp*Δ*rcsF*. Phospholipid samples were separated and visualised by TLC using a solvent mixture of methanol/ chloroform/ water with a ratio of 2:2:1.8 before being visualised by phosphomolybdic acid and charring.

388

389 The formation of ECA_{PG} is completed by attachment of linear ECA chains to diacylglycerol by
390 a phosphodiester bond through an unknown mechanism (Kuhn et al., 1983, Rai et al., 2021).
391 To determine the essentiality of ECA_{PG} we targeted synthesis of the donor molecule for ECA_{PG},
392 the phospholipid phosphatidylglycerol (Morris & Mitchell, 2023). The gene *pgsA* encodes
393 phosphatidylglycerophosphate synthase, which catalyses the first committed step in
394 biosynthesis of phosphatidylglycerol. However, loss of *pgsA* is lethal due to mislocalisation of
395 Braun's lipoprotein, Lpp, to the inner membrane and activation of the Rcs stress system.
396 These issues can be resolved by making an Δ*lpp*Δ*rcsF* mutant before constructing the Δ*pgsA*
397 mutation (Kikuchi et al., 2000, Rowlett et al., 2017, Suzuki et al., 2002). The
398 Δ*pgsA*Δ*surA*Δ*lpp*Δ*rcsF* quadruple mutant was viably constructed and the absence of
399 phosphatidylglycerol was confirmed by phospholipid extraction and thin layer chromatography
400 **(Fig 4D)**. This confirmed that the phospholipid donor for synthesis of ECA_{PG} is not essential in
401 the Δ*surA* mutant. Lastly, the gene *wzzE* is not required for the production of ECA_{LPS} or ECA_{PG},
402 but is required for production of ECA_{CYC} (Kajimura et al., 2005, Mitchell et al., 2018, Rai et al.,
403 2021). In the Δ*surA* TraDIS library, the gene *wzzE* contained a conditionally essential region
404 indicating that ECA_{CYC} is likely to be the form of ECA that is conditionally essential in a Δ*surA*
405 mutant **(Fig 4A)** (Mitchell et al., 2018).
406
407 ***meso*-DAP is essential in the absence of BamB, BamC or BamE**
408 The TraDIS data were searched for conditionally essential genes involved in cell envelope
409 biogenesis pathways other than LPS and ECA biosynthesis. The gene *dapF* was identified as
410 conditionally essential in Δ*bamB* and Δ*bamC* with visual inspection indicating decreased
411 insertions in *dapF* in Δ*bamE* **(Fig 5A)**. DapF converts LL-diaminopimelate (LL-DAP) to *meso*-
412 diaminopimelate (*meso*-DAP), which is then either decarboxylated to produce L-lysine by the
413 enzyme LysA or it is utilised in the biosynthesis of peptidoglycan (Dewey & Work, 1952,
414 Richaud et al., 1987). The gene *lysA* was non-essential in all strains tested, suggesting the
415 essentiality of *dapF* in these mutants is due to the requirement for *meso*-DAP in synthesis of
416 peptidoglycan **(Fig 5A and 5B)**.

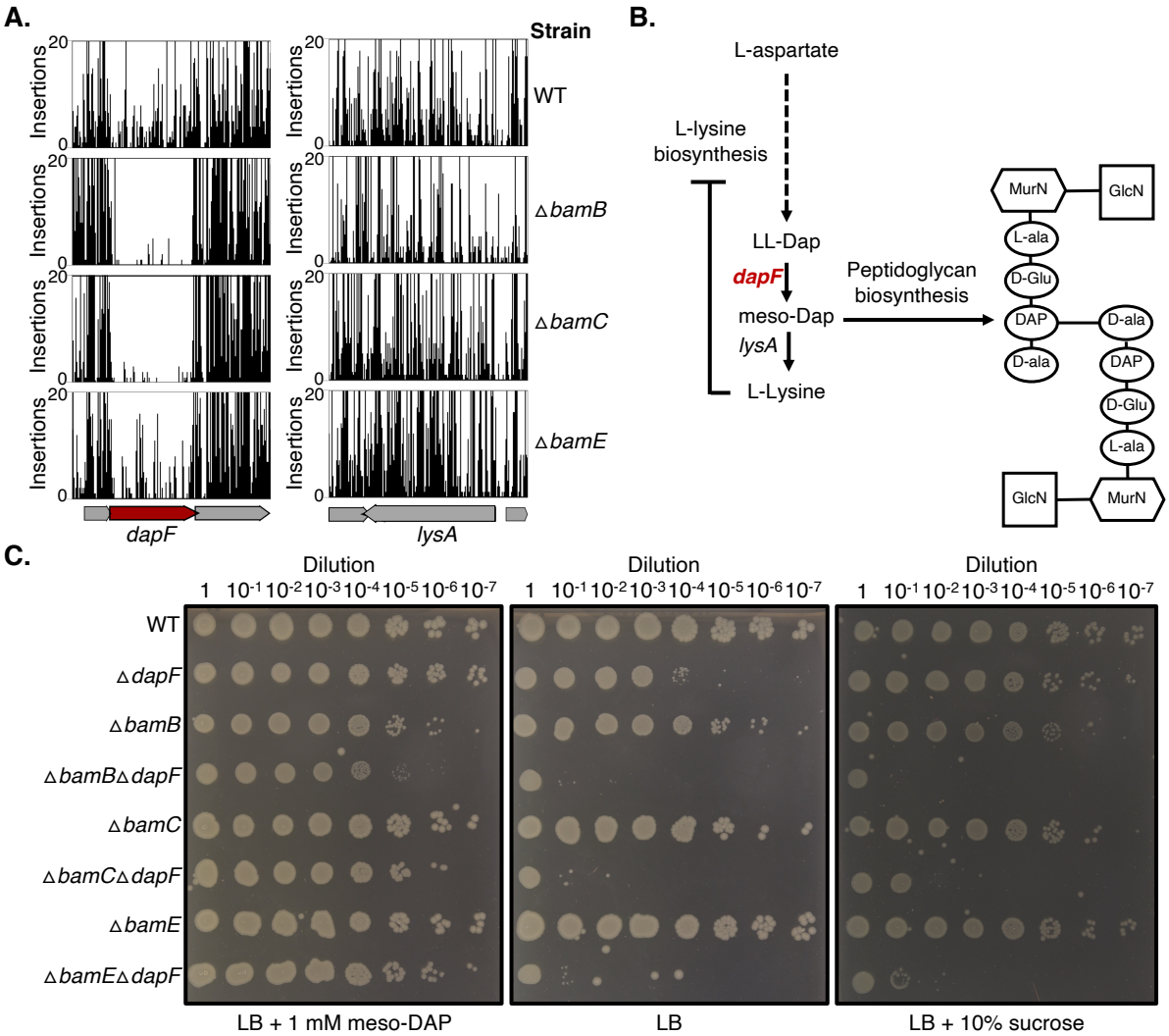

Figure 5 – *meso*-DAP containing peptidoglycan is essential in the absence of Bam accessory lipoproteins

A. Transposon insertions in the genes *dapF* and *lysA* in the parent or Δ*bamB*, Δ*bamC*, Δ*bamE* mutant TraDIS libraries. Transposon cut-off is set to 20. Essential genes are represented as red arrows. **B**. Schematic representation of the L-lysine biosynthesis pathway with the names of proteins labelled next to the reaction for which they are responsible. Conditionally essential proteins are labelled in red text. A schematic structure of *E. coli* peptidoglycan is shown with the site of *meso*-DAP incorporation shown. **C.** Efficiency of plating assay showing survival of the Δ*dapF*, Δ*bamB*, Δ*bamC*, Δ*bamE*, Δ*dapF*Δ*bamB*, Δ*dapF*Δ*bamC*, or Δ*dapF*Δ*bamE* mutants grown on LB with or without 1 mM *meso*-DAP or 10 % sucrose. Cells were grown overnight in LB supplemented with 1 mM *meso*DAP before being normalised to OD_{600} = 1.00 and serially diluted 1:10 before 2 μl was spotted on agar plates and incubated at 37°C overnight.

431 To validate the genetic interaction between Δ*dapF* and components of the Bam complex, the
432 *dapF* gene was knocked out in the BW25113 parent strain, Δ*bamB,* Δ*bamC* or Δ*bamE*
433 mutants. The double knockouts were selected in the presence of externally supplied *meso*-
434 DAP, which alleviated the loss of *dapF*. Cells were then grown in liquid media in the presence
435 of *meso*-DAP before being serially diluted in un-supplemented media and assayed for survival
436 in the presence or absence of *meso*-DAP by efficiency of plating assay. All strains grew
437 equally as well as the parent on LB agar supplemented with 1 mM *meso*-DAP, except for
438 Δ*bamB*Δ*dapF* which showed a minor decrease in CFU and colony size **(Fig 5C)**. However, in
439 the absence of *meso*-DAP the single Δ*dapF* mutant demonstrated a decrease in survival and
440 the double mutants were not viable **(Fig 5C)**. Lastly, considering that loss of DapF will lead to
441 a weaker peptidoglycan layer due to decreased crosslinks, we sought to negate the synthetic-
442 lethal phenotype by growth in the presence of sucrose as an osmoprotectant (Mengin-Lecreulx
443 et al., 1988, Mickiewicz et al., 2019). Unexpectedly, while the presence of 10% sucrose
444 enabled survival of the single *dapF* mutant to levels comparable to the parent, this was
445 insufficient to restore growth of the double mutant **(Fig 5C)**. This data demonstrates that
446 peptidoglycan structure is of increased importance in the absence of full Bam complex activity
447 and that this may not simply be due to structural support for the envelope.
448
449 **Regulation of DNA replication initiation is disrupted in the absence of BamB**
450 Our TraDIS experiment identified that in the Δ*bamB* dataset three KEGG pathways were
451 significantly enriched: “Homologous recombination”, “Mismatch repair” and “DNA replication”.
452 Bacterial DNA replication is mainly regulated at the initiation step by DnaA **(Fig 6A)**. The ATP-
453 bound form of this protein binds to DnaA boxes present at the chromosomal origin of
454 replication (*oriC*), with both high and low affinity, and directs replisome assembly (Jameson &
455 Wilkinson, 2017). Briefly, DnaA-ATP forms an oligomeric complex that facilitates unwinding of
456 the DNA strands, which in turn enables assembly of the replisome: the complex responsible
457 for replication of the bacterial chromosome. In *E. coli,* DnaA binding to its cognate DnaA boxes
458 is modulated by regulatory proteins. Negative regulation is achieved by two proteins. The

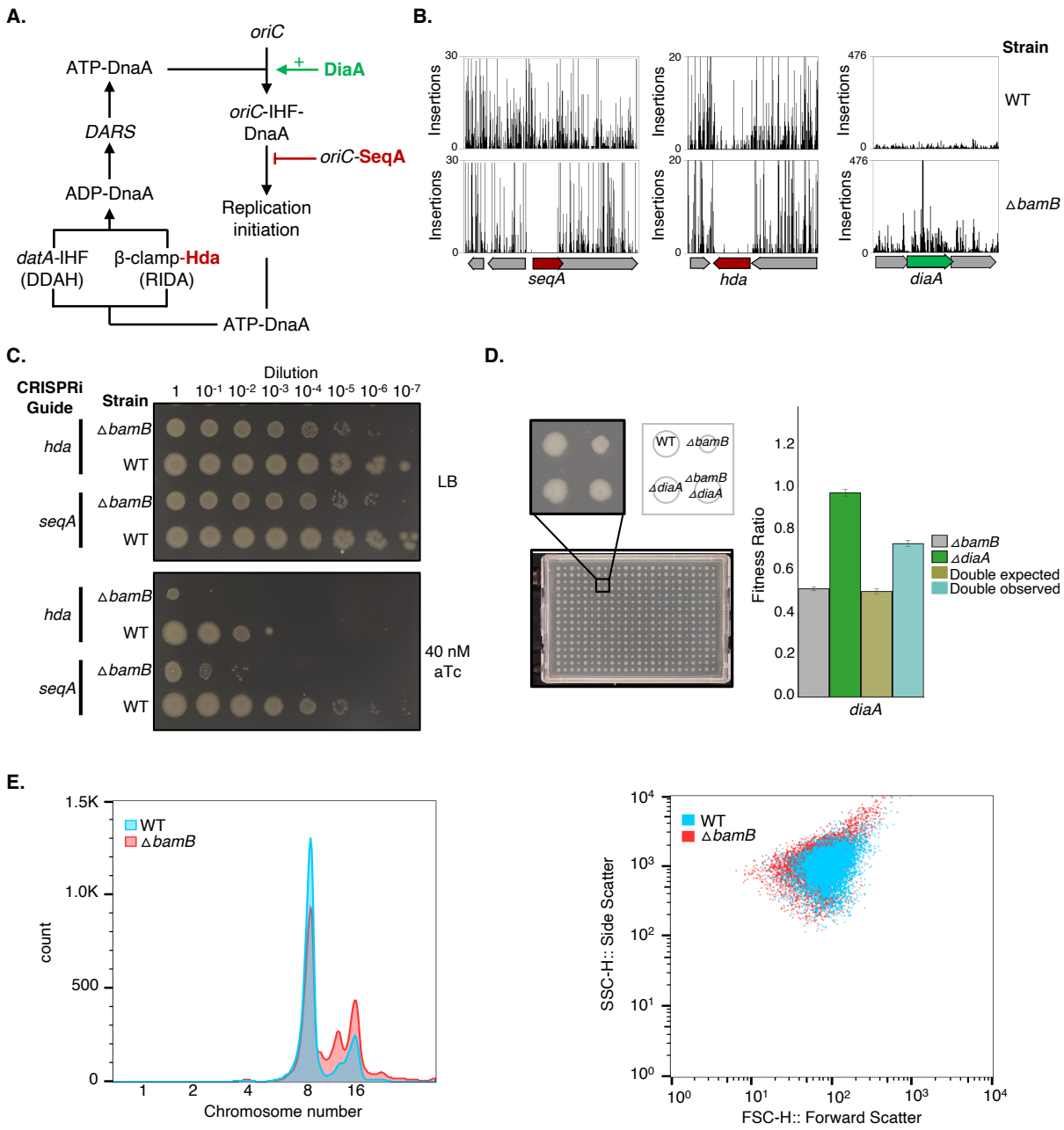

Figure 6 – Loss of BamB leads to changes in DNA replication control
A. Schematic representing DNA replication control in *E. coli*. DiaA stimulates initiation at the origin of replication, *oriC*, by DnaA. SeqA prevents premature reinitiation of replication. Hda acts together with the β-sliding clamp to hydrolyse ATP-bound DnaA by regulatory inactivation of DnaA (RIDA). This can also occur through *datA*-dependent DnaA-ATP hydrolysis (DDAH). **B.** Transposon insertions in the genes *hda*, *seqA* and *diaA* in the parent or Δ*bamB* mutant TraDIS libraries. Conditionally-essential genes are represented as red arrows and genes that increase fitness are in green. **C.** Efficiency of plating assay showing survival of the parent dCas9 expressing strain LC-E18 (WT) or Δ*bamB* mutant derivatives carrying the pSGRNA plasmid, which encodes CRISPRi guide RNA targeting either *seqA* or *hda*. Cells were grown on LB with or without 40 nM anhydro-tetracycline (aTc) to induce guide RNA expression. **D.** The *E. coli* BW25113 parent strain, single, or double Δ*bamB* and Δ*diaA* mutants were spotted on LB agar in 384-well format, in triplicate, and grown overnight at 37°C before being imaged. Fitness was calculated based on colony size and fitness ratios generated relative to the WT parent. **E.** Flow cytometry of *E. coli* LC-E18 cells grown in LB followed by replication run-out

assay. Forward scatter and side scatter are plotted with WT cell data indicated in blue and Δ*bamB* data points in red. Fluorescence is plotted and represents chromosomal content for each cell with chromosome numbers for each peak marked.

protein SeqA sequesters newly replicated origins, preventing premature reinitiation of replication (Lu et al., 1994, Torheim & Skarstad, 1999, von Freiesleben et al., 1994). The Hda protein works together with the β-sliding clamp to stimulate ATP hydrolysis of DnaA-ATP, which in the ADP-bound form is unable to promote initiation of DNA replication (Katayama et al., 1998, Kato & Katayama, 2001, Lu et al., 1994, Torheim & Skarstad, 1999, von Freiesleben et al., 1994). Positive regulation is facilitated by the DnaA initiator-associating factor, DiaA, which directly interacts with the N-terminal domain of DnaA to stimulate initiation at *oriC* (Ishida et al., 2004, Keyamura et al., 2007).

Analysis of the TraDIS data identified the genes *holC, holD, matP, seqA* and *hda* as conditionally essential in the Δ*bamB* mutant **(Table S1)**. Within this set of genes, we chose to focus on those with the clearest conditional essentiality from the TraDIS data, *hda* and *seqA.* Insertions within the negative regulator encoding genes, *seqA* and *hda*, led to decreased survival of Δ*bamB*. In contrast, increased fitness of Δ*bamB* was observed for cells containing disruptions of the positive regulator gene *diaA* **(Fig 6B)**. We confirmed the findings regarding the negative regulators by using CRISPRi. The *bamB::aph* allele was transferred into the dCas9 encoding strain *E. coli* LC-E18 and the kanamycin resistance marker was removed. The pSGRNA plasmid was used to express guide RNA targeting the *seqA* or *hda* genes in either the parent or Δ*bamB*. Expression of guide RNA targeting the *seqA* and *hda* genes led to significantly decreased survival of Δ*bamB* when compared to the parent strain, therefore confirming the observations made from TraDIS **(Fig 6C)**. The positive genetic interaction between *bamB* and *diaA* was confirmed by measuring fitness of the Δ*bamB*Δ*diaA* mutant compared to both single deletion mutants. Fitness of the double mutant was greater than the expected fitness for this strain **(Fig 6D)**.

504 Considering that loss of negative regulators of DNA replication initiation led to decreased
505 fitness of Δ*bamB*, and loss of the positive regulator increases fitness, we hypothesised that
506 the Δ*bamB* mutant may already have defective replication control. Therefore, we compared
507 chromosomal content of the wild-type and Δ*bamB* strain by using an established replication
508 run-out assay (Hawkins et al., 2016). Both strains were grown to early exponential phase
509 under conditions supporting fast cell growth (LB + 0.2% glucose), when cells contain multiple
510 replicating chromosomes. We reasoned that dysfunction of replication control is usually
511 exacerbated when cells grow with overlapping replication rounds. Next, cells were collected
512 and treated with rifampicin to inhibit further rounds of DNA replication initiation, and with
513 cephalexin to prevent cell division. Fixed cells were stained for DNA content with Sytox Green
514 and analysed by flow cytometry. The comparison of chromosomal copy number revealed a
515 higher proportion of cells with 16 chromosome copies for the Δ*bamB* mutant, which implies
516 that initiation of replication occurs earlier during the cell cycle in this strain relative to the
517 parent. Strikingly, a population of Δ*bamB* cells also displayed a number of chromosomes
518 deviating from the normally observed 2^n, as manifested by an additional peak between the 8
519 and 16 chromosome peaks. This is a hallmark of asynchronous DNA replication events, when
520 not all replication origins in the cell fire simultaneously **(Fig 6E, S7-9)**. Analysis of the other
521 Bam-accessory lipoprotein gene mutants and Δ*skp* by replication run-out assay revealed no
522 significant changes from the parent pattern **(Fig S10)**. Therefore, our results suggest that *E.*
523 *coli* over-initiates DNA replication in the absence of BamB. This is fully consistent with the
524 observations that Δ*bamB* cells are more fit if they lose the positive regulator of DNA replication,
525 DiaA, but have decreased fitness in the absence of the negative regulators SeqA and Hda.
526

527 **OMP trafficking protein conservation varies throughout Gram-negative bacteria**

528 The data presented here demonstrate that in *E. coli,* the Bam-associated proteins likely have
529 specialised functions that are potentially coordinated with LPS structure, the presence and
530 form of ECA, peptidoglycan biogenesis and DNA replication control. Considering these

531 results, we revisited the evolutionary conservation of Bam complex subunits and the
532 periplasmic chaperone pathway proteins (Webb et al., 2012). Reference genomes for a
533 diverse range of Gram-negative bacterial representative strains were used to search for
534 sequences coding the Bam complex subunits (as observed in *E. coli*) or the chaperone
535 pathway proteins SurA, Skp and DegP. A combination of Prokka annotation, hmmsearch,
536 SignalP 6.0 (Teufel et al., 2022) and manual curation were used to generate a neighbour
537 joining tree with a heat map of gene counts in each organism **(Fig 7)**. While we found broad
538 conservation of all query proteins within the gamma- and beta-proteobacteria, there are some
539 notable exceptions. The BamB and BamC lipoproteins are not conserved within two species
540 of the aphid endosymbiont *Buchnera aphidicola* and the data confirm previous unpublished
541 observations that a strain of *B. aphidicola*, (subspecies *Baizongia pistaciae*) appears to have
542 entirely lost genes encoding the Bam complex (Malinverni & Silhavy, 2011). Likely this is due
543 to the strain containing only a few OMPs, therefore no longer requiring a dedicated OMP
544 assembly machinery.
545 Outside of the gamma- and beta-proteobacteria requirement for the Bam-associated proteins
546 appears to be diverse. The lipoproteins BamB and BamC are largely absent in the alpha-
547 proteobacteria, and the epsilon-proteobacteria only encode the core components BamA and
548 BamD, demonstrating reductive evolution. This minimalist form of the Bam complex is
549 sufficient for OMP insertion, which is likely due to reduced β-barrel complexity as observed in
550 *Helicobacter pylori* (Webb et al., 2017). This indicates that the specialised roles these proteins
551 may play in *E. coli* are not required in these organisms **(Fig 7)**. While there is diversity in the
552 presence or absence of these proteins in the organisms analysed, multiple copies of some
553 components were also identified. In particular, we found that *Pseudomonas putida* encodes
554 two copies of BamA, BamE and SurA. Outside of the gamma-proteobacteria there are
555 numerous examples of species encoding multiple copies of BamA, particularly within the
556 alpha-proteobacteria, such as the plant pathogen *Agrobacterium tumefaciens* **(Fig 7)**. These
557 copies may play specialised roles in folding and inserting specific cargo, or they may alleviate
558 an increased requirement for OMP insertion in these organisms. Taken together, the diverse

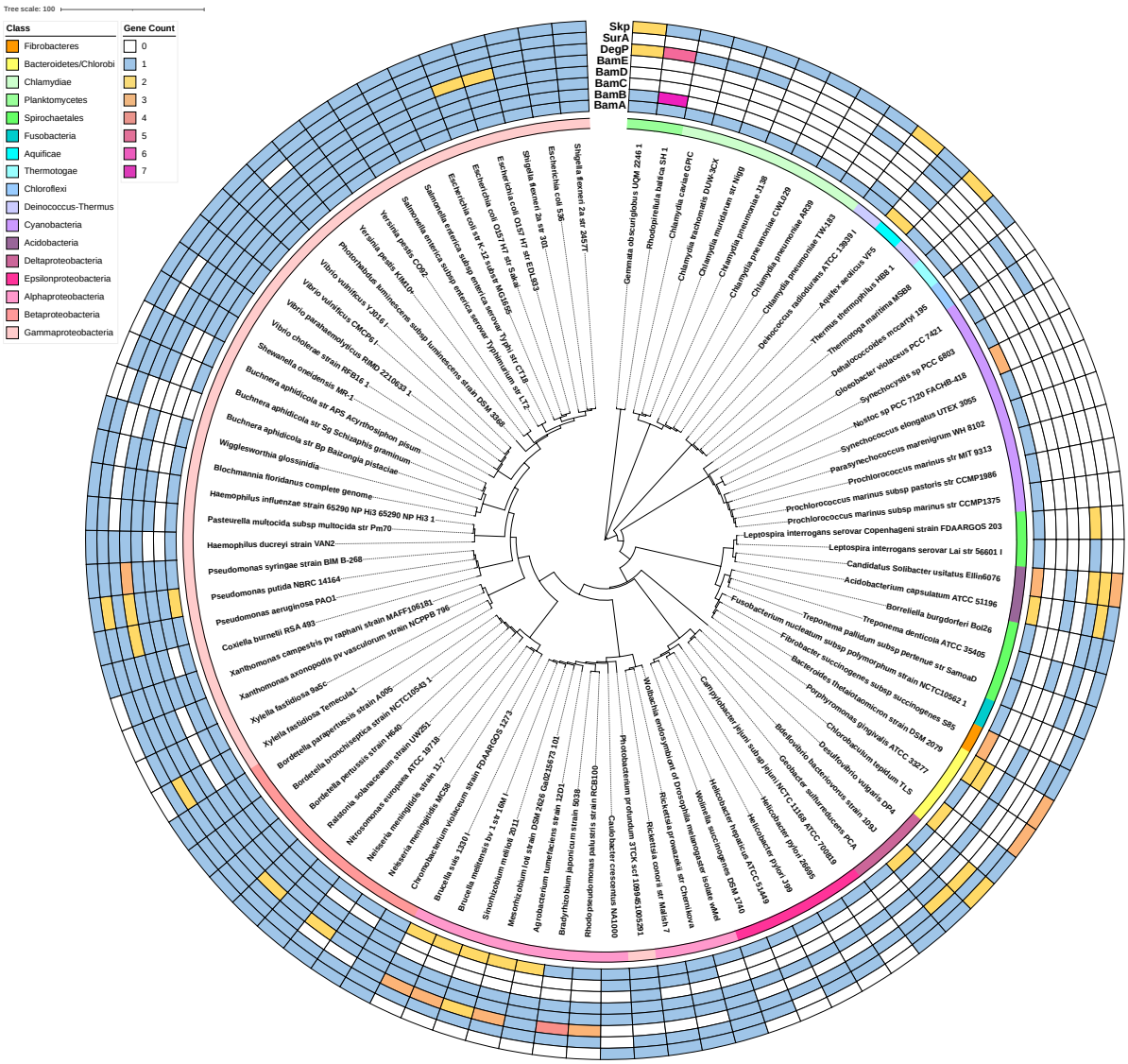

Figure 7 – Conservation analysis of Bam-associated proteins in Gram-negative bacteria Conservation of the BamB, BamC, BamE, SurA, DegP and Skp proteins among key Gram-negative bacterial species represented by a presence/absence map plotted onto a phylogenetic tree generated with iTOL (Letunic & Bork, 2021). Gene count in each species is represented by coloured boxes.

566 range of Bam complex subunit compositions within Gram-negative bacteria support the
567 hypothesis that the Bam-associated proteins likely play specialised roles that vary in each
568 organism.
569
570 **Discussion**
571 The Bam complex has been identified as a potential target for antimicrobials, with several new
572 inhibitors of this essential outer membrane biogenesis machine being identified recently
573 (Steenhuis et al., 2021). However, despite this focus as an important new avenue for drug
574 discovery, and recent advances in understanding the mechanism by which the Bam complex
575 folds and inserts OMPs into the outer membrane (Doyle et al., 2022, Tomasek et al., 2020),
576 we still do not fully understand the roles of the Bam-associated proteins in *E. coli*. We also do
577 not understand why the complex appears to be modular, with subunits being differentially
578 conserved throughout Gram-negative bacteria as shown through our analysis and those done
579 previously **(Fig 7)** (Webb et al., 2012). Constituent parts of the outer membrane such as
580 phospholipid species, type of LPS, O-antigen, ECA, lipoprotein content, and variety/flux of the
581 unfolded OMP proteins can vary across bacterial species (Simpson & Trent, 2019, Valvano,
582 2022). Such variation would likely result in significant differences in the biophysical constraints
583 of the membrane environment in which the Bam complex must operate. In addition, there is
584 likely to be differing requirements for the chaperone pathway proteins depending on the pool
585 of client OMPs. Considering that Skp and SurA have been shown to act on different unfolded
586 states of OmpC, with Skp likely being more important during stress conditions, the
587 environmental conditions experienced by each species could also dictate the requirement for
588 each OMP chaperone (Li et al., 2018). Together, this strongly suggests that each accessory
589 lipoprotein is likely to have specialised functions and that the chaperone proteins are unlikely
590 to be truly functionally redundant. This is supported by our phenotypic profiling of knockout
591 strains. Should each of the accessory lipoproteins merely contribute to overall activity of the
592 Bam complex, and if there is true redundancy in the chaperone pathway, then we would expect
593 that the knockout strains should phenocopy each other. However, we found this not to be the

594 case **(Fig 1)**. Our TraDIS analysis also supports this conclusion as we saw a large number of
595 unique conditionally essential genes for each mutant **(Fig 2)**.
596
597 *Role of the outer membrane lipid environment for OMP insertion*
598 The Bam complex must function within the constraints of the outer membrane lipid
599 environment, therefore OMP biogenesis is likely to be affected by changes to outer membrane
600 lipids. Indeed, we found conditional essentiality between genes involved in LPS inner core
601 biogenesis and either *bamB*, *surA* or *degP*. Complete truncation of the LPS inner core by
602 disruption of the last enzyme in the heptose biosynthesis pathway has previously been
603 demonstrated to increase membrane fluidity and lead to decreased Bam complex activity
604 (Storek et al., 2019). We confirmed this observation and further demonstrate that the changes
605 to membrane fluidity are of graded severity relating to the severity of LPS inner core truncation.
606 This in turn leads to a graded impact on Bam complex activity **(Fig 3)**. The Δ*bamB,* Δ*surA* and
607 Δ*degP* knockout strains have the most severe phenotypes within the set of strains tested here
608 (**Fig 1)**. Also, loss of BamB, SurA or DegP each leads to OMP assembly defects, decreased
609 numbers of folded OMPs in the outer membrane, and accumulation of unfolded OMPs in the
610 periplasm (Charlson et al., 2006, Krojer et al., 2008, Lazar & Kolter, 1996, Rouvière & Gross,
611 1996, Wu et al., 2005). We hypothesise that the negative effect of increased membrane fluidity
612 on the Bam complex in combination with decreased levels of OMP assembly in the absence
613 of BamB, SurA or DegP leads to OMP assembly levels that are too low to sustain cell viability.
614 This is of particular significance when considering the variation in LPS structure seen between
615 different strains, and the LPS modifications available, which could affect the level of Bam
616 activity and influence the conservation of each Bam-associated protein (Simpson & Trent,
617 2019, Valvano, 2022).
618
619 *A role for ECA_{cyc} in amelioration of periplasmic protein folding stress?*

620 The carbohydrate antigen ECA consists of three repeating sugars, is widely conserved
621 amongst the *Enterobacterales*, and is produced in three forms that are either surface exposed
622 (ECA_{LPS} and ECA_{PG}) or periplasmically localised (ECA_{CYC}). The invariant nature of the antigen
623 suggests it has an important undiscovered function, however the role of ECA in outer
624 membrane biology remains unknown (Rai & Mitchell, 2020). We identified that ECA biogenesis
625 becomes essential in the absence of the chaperone SurA **(Fig 4A)**. Production of ECA
626 requires the lipid carrier undecaprenyl phosphate (Und-P), which is limited in the cell and
627 utilised in numerous metabolic reactions including the production of peptidoglycan, capsule,
628 O-antigen and membrane-derived oligosaccharides. Disruption of ECA biogenesis can cause
629 stress on these other pathways due to Und-P sequestration in ECA dead-end intermediates
630 (Jorgenson et al., 2016, Mitchell et al., 2018, Rai & Mitchell, 2020). However, the first gene in
631 the ECA pathway is conditionally essential in the absence of SurA **(Fig 4A)**, therefore the
632 effects are unlikely due to stress on the Und-P pool. Instead, we showed that the
633 periplasmically localised form, ECA_{cyc}, is essential in the absence of SurA **(Fig 4)**. It is possible
634 that ECA_{cyc} might help stabilise the outer membrane of a Δ*surA* mutant, as it has been shown
635 to suppress the envelope permeability defect of a Δ*yhdP* mutant. However, the molecular
636 details of this suppression are yet to be discovered (Mitchell et al., 2018). Alternatively,
637 disruption of ECA biosynthesis activates the Cpx, Rcs, and σ^E stress responses, which in
638 addition to activation of these pathways by the loss of SurA could led to excessive activation
639 of stress responses that are lethal to the cell (Castanié-Cornet et al., 2006, Danese et al.,
640 1998, Jorgenson et al., 2016). Finally, ECA_{cyc} could be performing a chaperone function
641 directly, however this would require *in vitro* assays of protein aggregation with purified
642 products for proof.
643
644 *Coordination of OMP biogenesis with peptidoglycan biosynthesis*
645 In order to ensure successful cell growth and division, activity of the Bam complex must be
646 coordinated with biogenesis of the peptidoglycan layer. Our TraDIS analysis identified that in

647 the Δ*bamB,* Δ*bamC* and Δ*bamE* mutants, the gene *dapF* was essential **(Fig 5A)**. The DapF
648 enzyme is responsible for synthesis of the peptidoglycan stem-peptide component *meso*-DAP.
649 The single and double mutants could be rescued by exogenous *meso*-DAP, however only the
650 single *dapF* mutant could be rescued by the osmo-protectant sucrose, which is sufficient to
651 allow survival during disruption of peptidoglycan biogenesis **(Fig 5B)** (Mickiewicz et al., 2019).
652 Loss of *meso*-DAP in the single *dapF* mutant leads to accumulation of LL-DAP, which is
653 incorporated into peptidoglycan and leads to decreased crosslinking (Mengin-Lecreulx et al.,
654 1988, Richaud et al., 1987). In the Δ*dapF* mutant the peptidoglycan layer would be able to
655 withstand less mechanical load due to decreased crosslinking. This decreased mechanical
656 strength, in combination with the reduced capacity for load bearing by the outer membrane in
657 the Bam complex mutants, means that the cells are unlikely to withstand osmotic stress (Rojas
658 et al., 2018). However, while this may be true for Δ*bamB* and Δ*bamE* mutants, there are no
659 strong phenotypic effects for Δ*bamC* (**Fig 1)** (Nichols et al., 2011). Also, the loss of BamC has
660 only a slight effect on the membrane permeability barrier, no detectable changes to the outer
661 membrane proteome, and no effect on OMP folding in an *in vitro* assay (Thewasano et al., Wu
662 et al., 2005). Consequently, the synthetic lethality between *dapF* and *bamC* is unlikely to be
663 due to osmotic stress tolerance, as could be the case for the other mutants.
664 It has recently been demonstrated that the Bam complex preferentially inserts OMPs at the
665 cell division site and that this is coordinated by interaction with the peptidoglycan layer (Mamou
666 et al., 2022). While all of the Bam complex proteins were shown to interact with peptidoglycan
667 *in vitro*, only BamA and BamC were found to interact with peptidoglycan in whole cells when
668 analysed by crosslinking and pull-down assays (Mamou et al., 2022). Considering the
669 interaction of mature peptidoglycan with BamC and the altered peptidoglycan structure in the
670 Δ*dapF* strain (Mengin-Lecreulx et al., 1988, Richaud et al., 1987), we hypothesise that BamC
671 might facilitate coordination between the Bam complex and peptidoglycan biosynthesis,
672 however this requires further investigation.
673

674 *Link between OMP biogenesis and DNA replication control*

675 Not only must envelope biogenesis processes be coordinated with each other, but synthesis
676 of the envelope must be coordinated with cell growth and cell division. Experimental evidence
677 suggests that both DNA replication control (Si et al., 2017, Wallden et al., 2016) and the rate
678 of cell surface synthesis are coupled to cell volume (Harris & Theriot, 2016). This provides the
679 rationale for existence of mechanisms that modulate DNA replication rate in response to cell
680 envelope synthesis perturbation. Here we demonstrated that in the absence of BamB, cells
681 over-initiate DNA replication and that synchrony of replication initiation at multiple origins is
682 compromised **(Fig 6E)**. Also, our phenotypic screen revealed that Δ*bamB* has increased
683 fitness at sub-optimal growth temperatures. This would lead to slower growth, a factor that is
684 known to alleviate some DNA replication control defects, such as those arising from loss of
685 SeqA (Lu et al., 1994). In addition, we found that the Δ*bamB* mutant is sensitive to
686 hydroxyurea, which specifically inhibits ribonucleotide reductase and leads to depletion of the
687 cellular dNTPs pool, replication fork arrest and genomic instability **(Fig 1)** (Davies et al., 2009,
688 Nakayashiki & Mori, 2013). Similarly to Δ*bamB*, mutants that also over-initiate replication, such
689 as *seqA* mutants, are also sensitive to hydroxyurea (Sutera & Lovett, 2006).

690 Led by our TraDIS results, we confirmed that *seqA* and *hda* are essential in the Δ*bamB* mutant
691 **(Fig 6)** and that this is likely due to over-initiation of DNA replication, which can be caused by
692 all three of these mutations (Camara et al., 2005, Lu et al., 1994, von Freiesleben et al., 1994).
693 SeqA is required to prevent premature re-initiation of replication through sequestration of
694 newly replicated GATC sites within oriC, whereas Hda prevents re-initiation of replication
695 through regulatory inactivation of DnaA (RIDA), in combination with the β-sliding clamp of DNA
696 polymerase (Camara et al., 2003, Lu et al., 1994). Interestingly, we also identified that two
697 components of the β-sliding clamp loader complex, HolC and HolD, become essential in the
698 Δ*bamB* mutant **(Table S1)**. These proteins contribute towards activity of the clamp loader.
699 Therefore, the synthetic lethality could be due to decreased RIDA and over-initiation of DNA
700 replication, as observed for the *hda* mutant (Cooper et al., 2021, Katayama et al., 1998).

701 This is the first link between the Bam complex and DNA replication control, however links
702 between the envelope and DNA replication have been observed previously. In order to initiate
703 DNA replication, the DnaA protein must be in the ATP-bound form and regeneration of DnaA-
704 ATP from the ADP-bound form is facilitated by interaction with phospholipids. (Garner et al.,
705 1998, Sekimizu & Kornberg, 1988). DNA replication control and envelope biogenesis are also
706 linked by the SeqA protein, which has been associated to the purified outer membrane fraction
707 in a cell-cycle dependent manner, however the mechanism remains unclear (d'Alençon et al.,
708 1999). In addition, disrupted origin/terminus ratios in *seqA* mutant strains are suppressed by
709 mutations in the *waaG, waaQ* and waa*P* genes, which are responsible for addition of the outer
710 core of LPS, heptose III addition to the inner core and phosphorylation of heptose II of the LPS
711 inner core, respectively (Rotman et al., 2009, Valvano, 2022). Interestingly, the Δ*bamB* mutant
712 is also sensitive to changes in membrane fluidity brought about by LPS modifications that map
713 to the inner core **(Fig 3)**.
714 We also identified that insertions in the *diaA* gene, which encodes a positive regulator of DNA
715 replication initiation, can suppress Δ*bamB*. The *diaA* gene is part of a conserved four gene
716 cluster that also encodes LpoA - a regulator of peptidoglycan biogenesis, YraN - a protein of
717 unknown function, and DolP - a cell-division site localised outer membrane lipoprotein shown
718 to interact with the Bam complex (Bryant et al., 2020, Ranava et al., 2021). The genes in this
719 cluster all appear to be linked to regulating cellular growth processes such as peptidoglycan
720 biogenesis, OMP insertion into the outer membrane and DNA replication. This is of particular
721 interest considering our data demonstrate potential coordination of these processes, which is
722 essential to ensure efficient growth and survival during cell division.
723 Together, our data demonstrate that the Bam-associated proteins have specialised roles in
724 the cell and highlights potential future targets to understand these roles. We provide further
725 evidence that OMP transport, folding and insertion is affected by, and potentially coordinated
726 with, peptidoglycan and LPS structure. We also show that Bam function is correlated with DNA
727 replication control and highlight the BamB lipoprotein, outer membrane fluidity and LPS

structure as a potential route through which this could occur. This provides a strong direction for further study to understand this coordination.

Acknowledgments

This work was supported by a UKRI Future Leaders Fellowship [MR/V027204/1] and a Springboard Award [SBF005\1112] to Manuel Banzhaf. The work was also funded by the National Science Centre Poland [UMO-2014/13/B/NZ2/01139] (awarded to Monika Glinkowska), the KAUST baseline fund [BAS/1/1108-01-01] awarded to Danesh Moradigaravand who is a member of the KAUST Smart-Health initiative, and the EU ITN Train2Target [721484] that funded training of Kara Staunton.

Conflict of interest

The authors declare that they have no conflict of interest

741 **Supplementary figures**

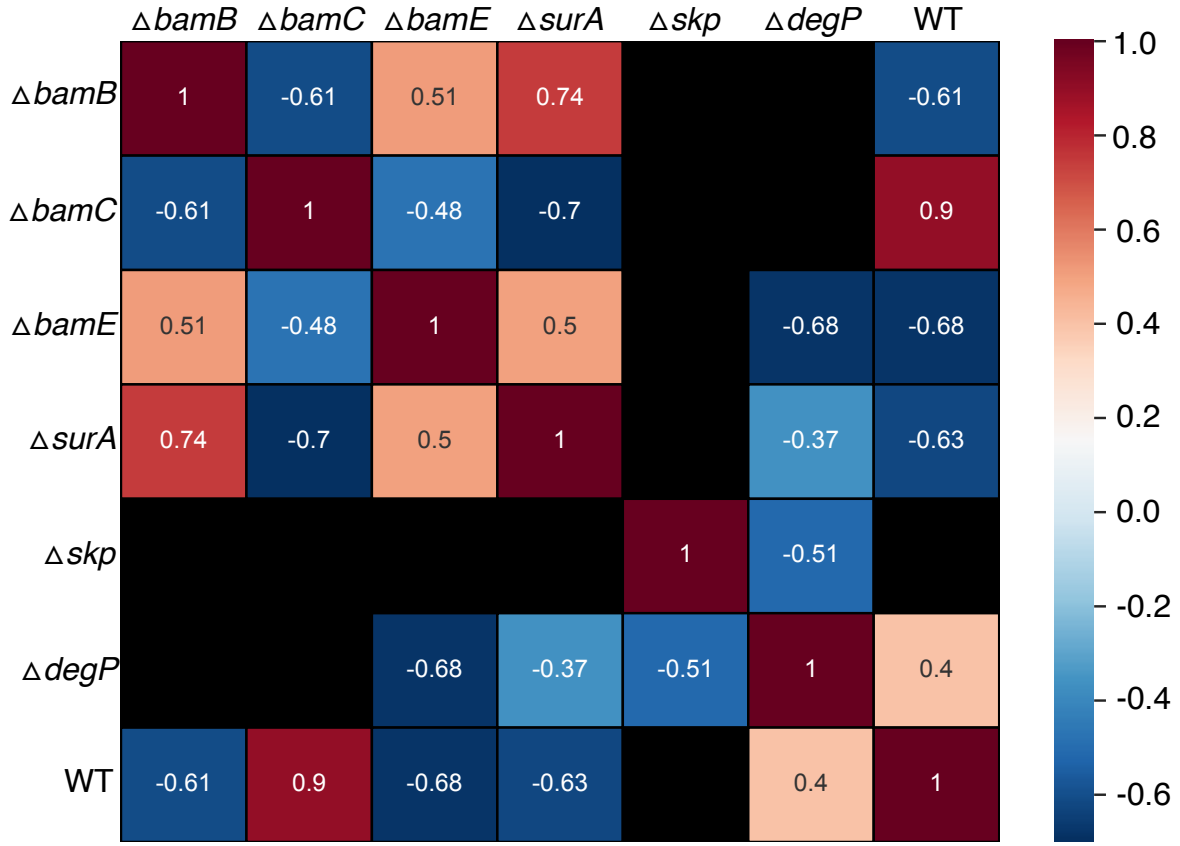

742

743 **Figure S1 – Correlation of phenotypic profiles**
744 Heatmap of Pearson correlation coefficients for each pair of strain phenotypic profiles.
745 Correlation of fitness ratios for each strain was assessed by calculating the Pearson
746 correlation coefficient for averaged fitness scores across replicates using Python before being
747 plotted as a heatmap. Black squares indicate a p-value ≥0.05 meaning the correlation
748 coefficient achieved was not statistically significant.

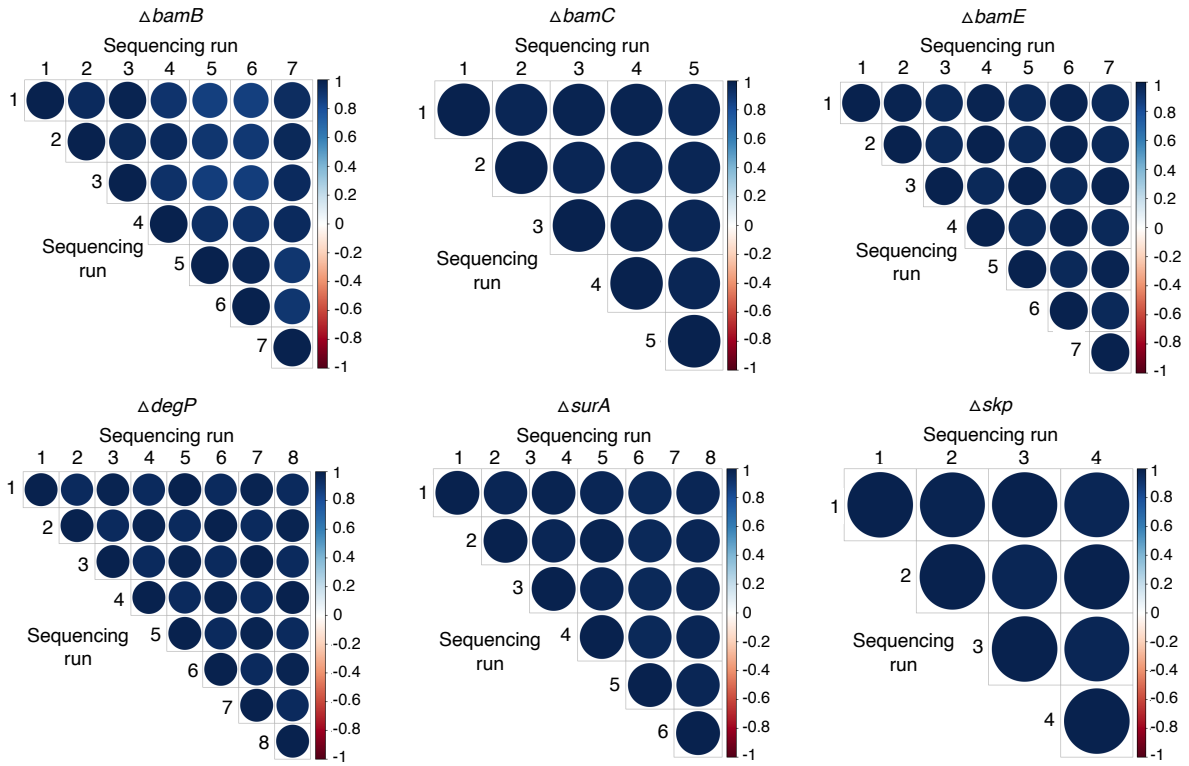

Figure S2 – Reproducibility across TraDIS library sequencing runs
Correlogram of insertion indexes between individual sequencing runs for each TraDIS library. The colour and size of the bubbles correspond to the strength of the Pearson correlation coefficient between the indices for the same genes across the runs. The blue colour represents positive correlation.

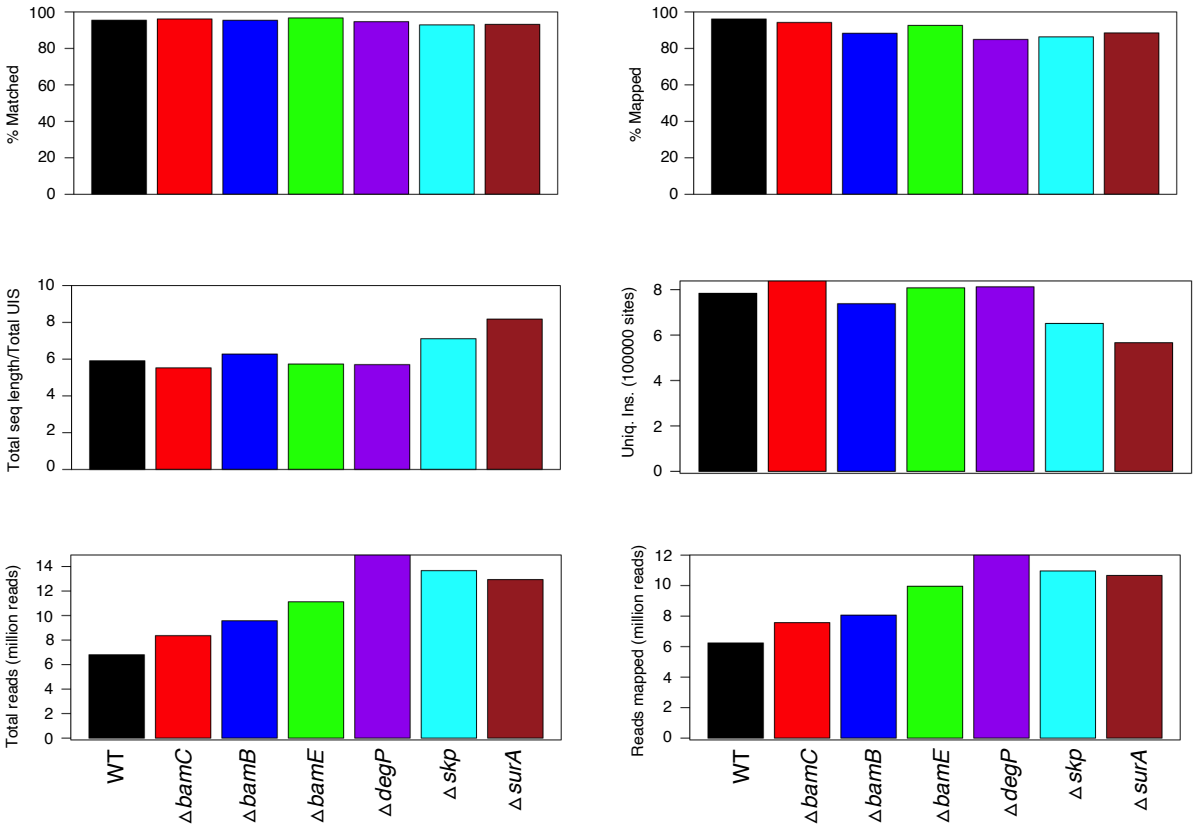

Figure S3 – Transposon library construction metrics
TraDIS library construction metrics showing the percentage of sequencing reads that matched the transposon tag and that mapped to the chromosome. Total sequencing length as a function of total unique insertion sites, the total number of unique insertion sites for each sample, total number of sequencing reads, and the number of reads that mapped are also shown.

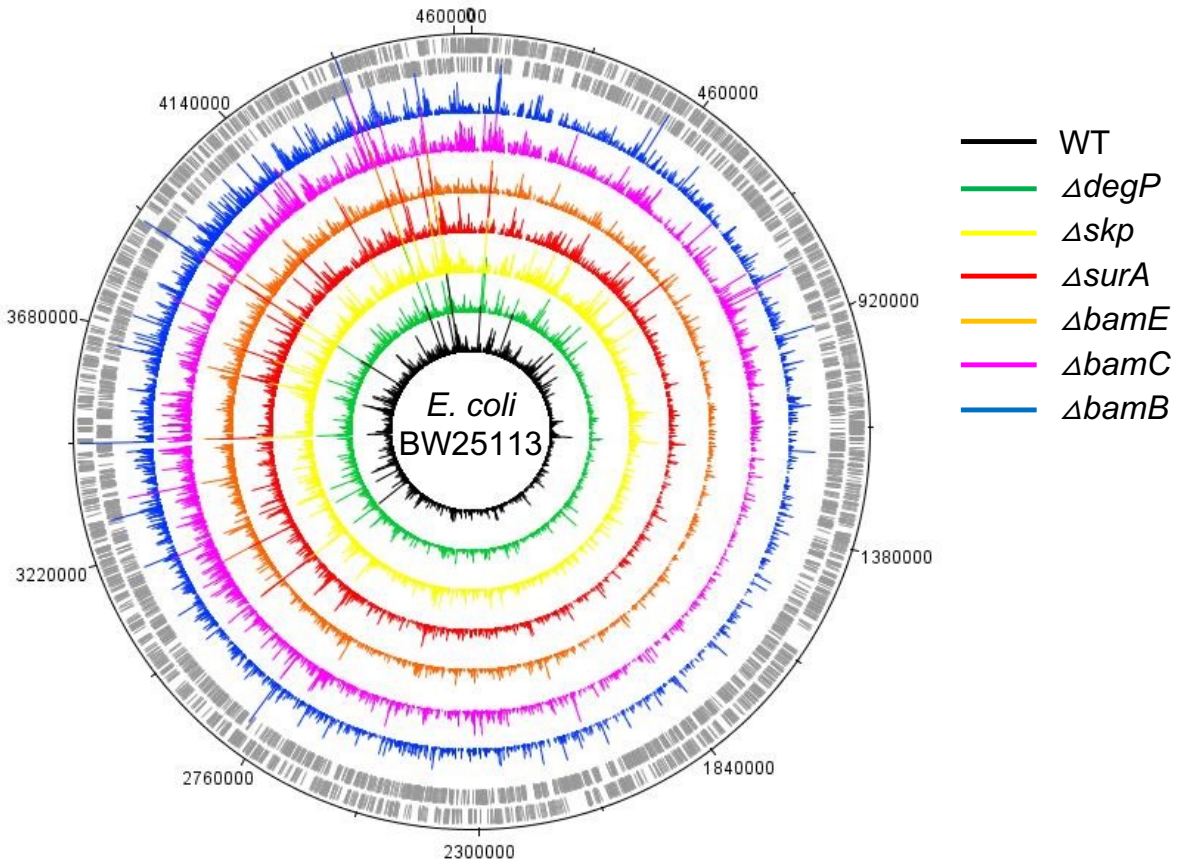

765
766 **Figure S4 – Circular plots of transposon insertion density in TraDIS libraries.** Circular
767 plot of transposon insertion sites in the parent BW25113 (WT), Δ*degP,* Δ*skp,* Δ*surA,* Δ*bamE*,
768 Δ*bamC*, Δ*bamB* TraDIS libraries, listed from innermost tracks outwards, generated using
769 DNAPlotter. The outermost track marks the BW25113 genome in base pairs with the inner
770 grey bar tracks corresponding to sense and antisense CDS.
771

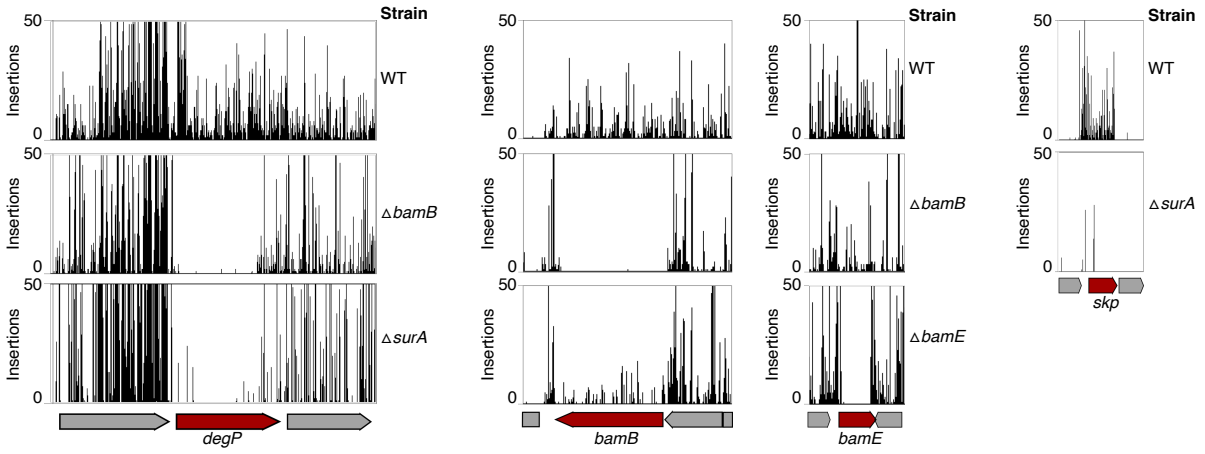

Figure S5 – Examples of known synthetic lethal interactions
Transposon insertions in the genes *degP*, *skp*, *bamB* or *bamE* in the WT parent strain, Δ*bamB*, or Δ*surA* mutant TraDIS libraries. Conditionally-essential genes are represented as red arrows, non-essential genes are represented by grey arrows. Transposon cut-off is set to 50.

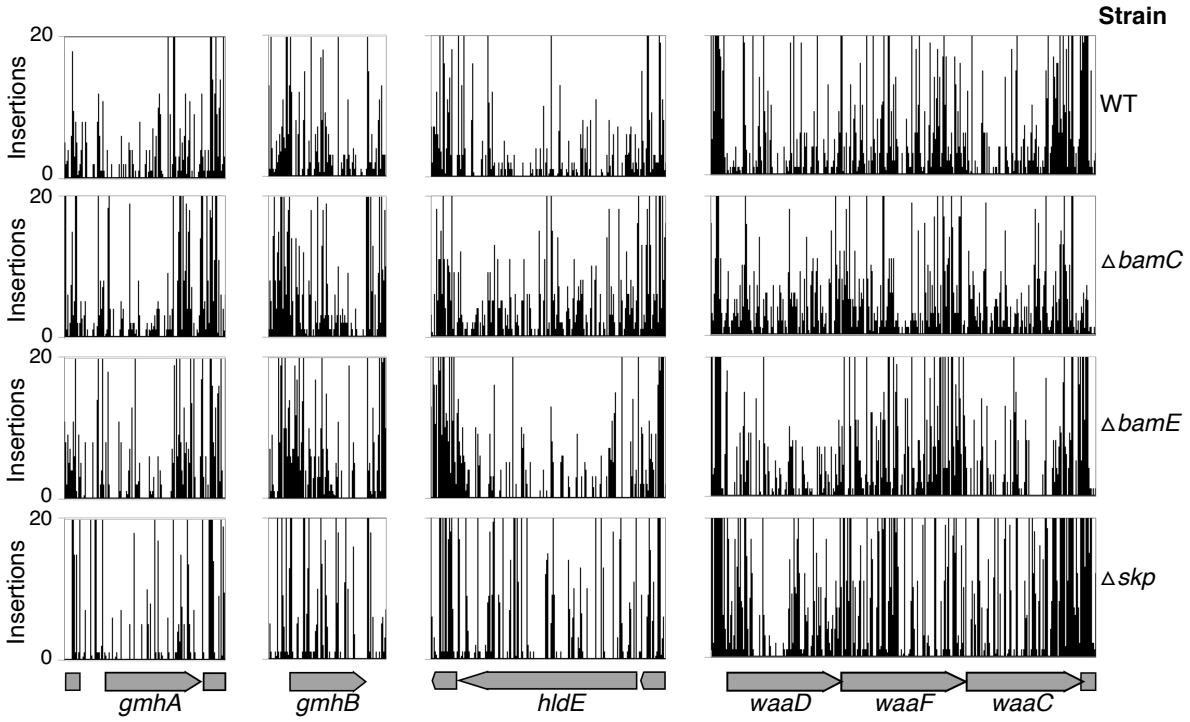

Figure S6 – Transposon insertions in genes required for heptose biosynthesis in the Δ*bamC,* Δ*bamE* and Δ*skp* TraDIS libraries

Transposon insertions in the genes *gmhA*, *gmhB*, *hldE, waaD, waaC,* and *waaF* in the parent, Δ*bamC,* Δ*bamE* and Δ*skp* TraDIS libraries. Transposon cut-off is set to 20. Essential genes are represented as red arrows and non-essential genes are represented by grey arrows.

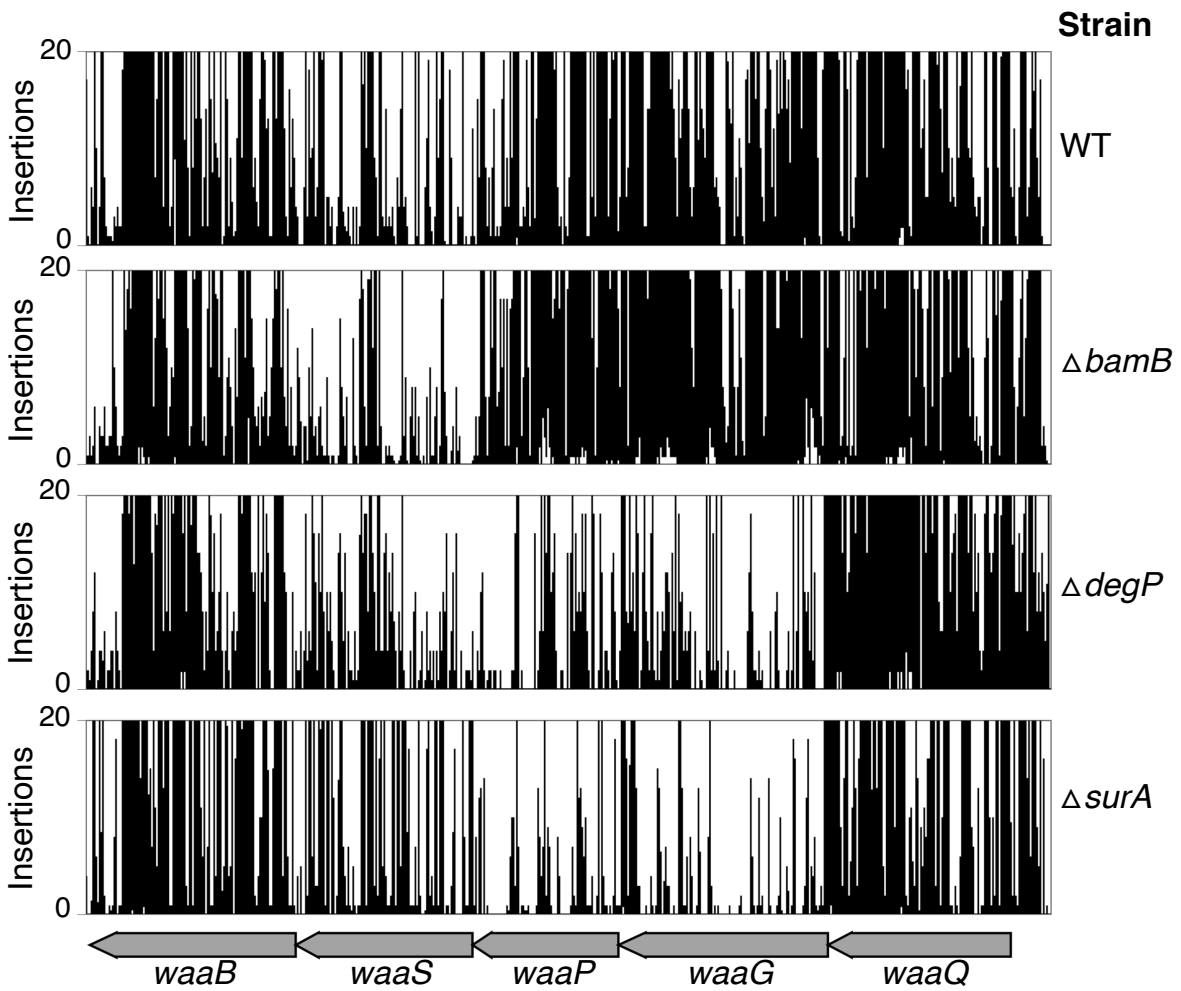

785

786 **Figure S7 – Transposon insertions in the *waaG* and *waaP* genes in the WT, Δ*bamB,***
787 **Δ*degP* and Δ*surA* TraDIS libraries**
788 Transposon insertions in the genes *waaB, waaS, waaP, waaG* and *waaQ* in the parent,
789 Δ*bamB,* Δ*degP* and Δ*surA* TraDIS libraries. Transposon cut-off is set to 20. Genes are
790 represented by grey arrows.
791

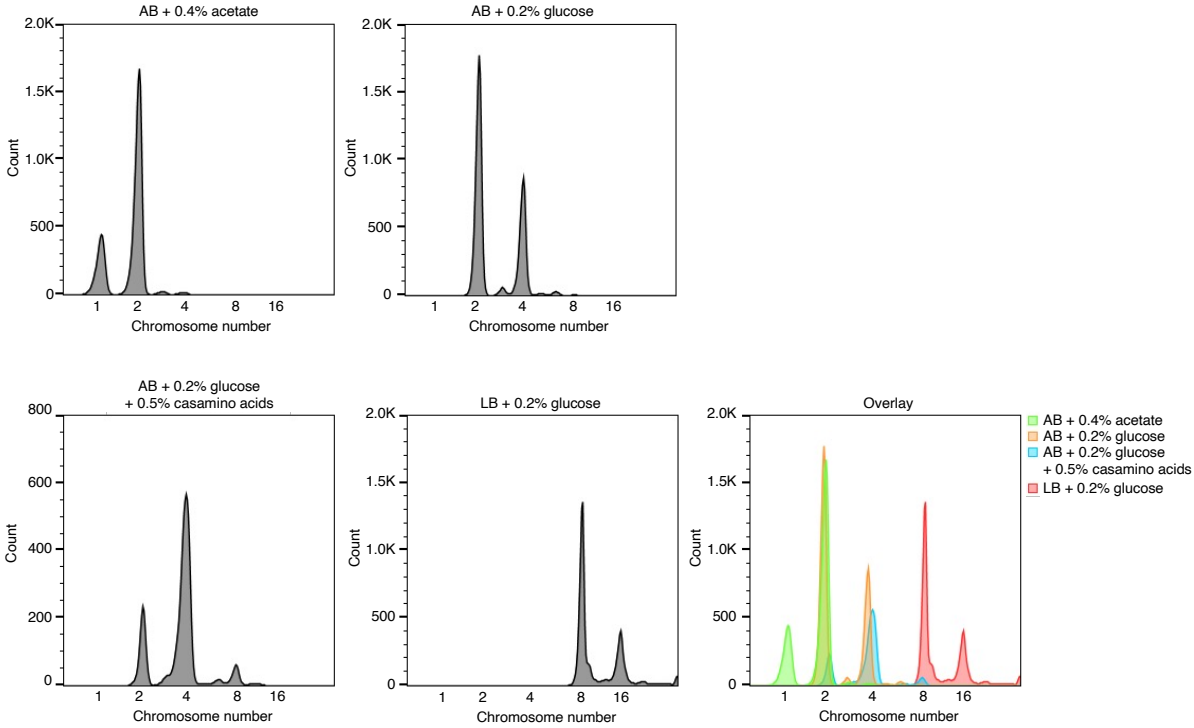

Figure S8 – Replication run-out assay standards

Flow cytometry of *E. coli* MG1655 cells grown in media supporting different growth rates followed by replication run-out assay. Cells were grown in AB minimal medium supplemented with either 0.4% acetate, 0.2% glucose, or 0.2% glucose + 0.5% casamino acids, or LB supplemented 0.2% glucose at 37°C with aeration before being treated with rifampicin, cephalexin and stained with Sytox Green. Fluorescence is plotted and represents chromosomal content for each cell with chromosome numbers for each peak marked. An overlay of the separate data panels is presented.

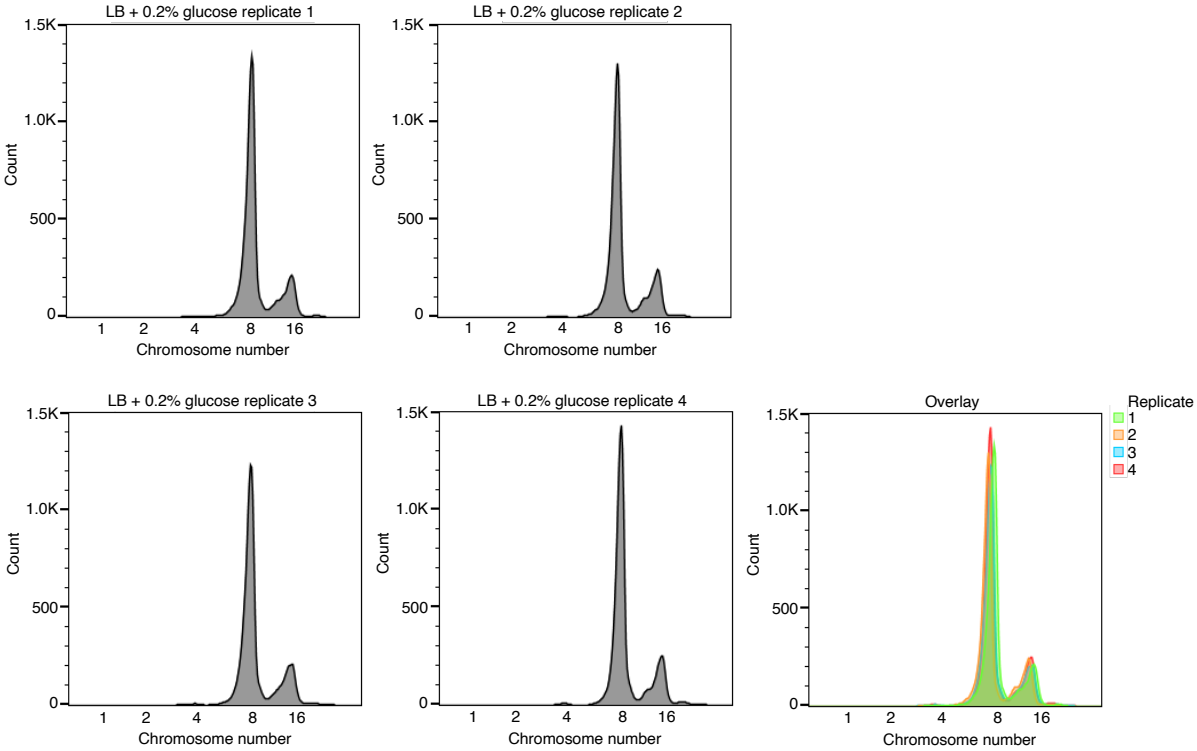

Figure S9 – Reproducibility of replication run-out assays for the parent strain
Flow cytometry of *E. coli* LCE-18 cells grown in LB supplemented with 0.2% glucose at 37°C with aeration before being treated with rifampicin, cephalexin and stained with Sytox Green. Fluorescence is plotted and represents chromosomal content for each cell with chromosome numbers for each peak marked. Each experiment was repeated on 4 separate occasions and an overlay of the separate data panels is presented.

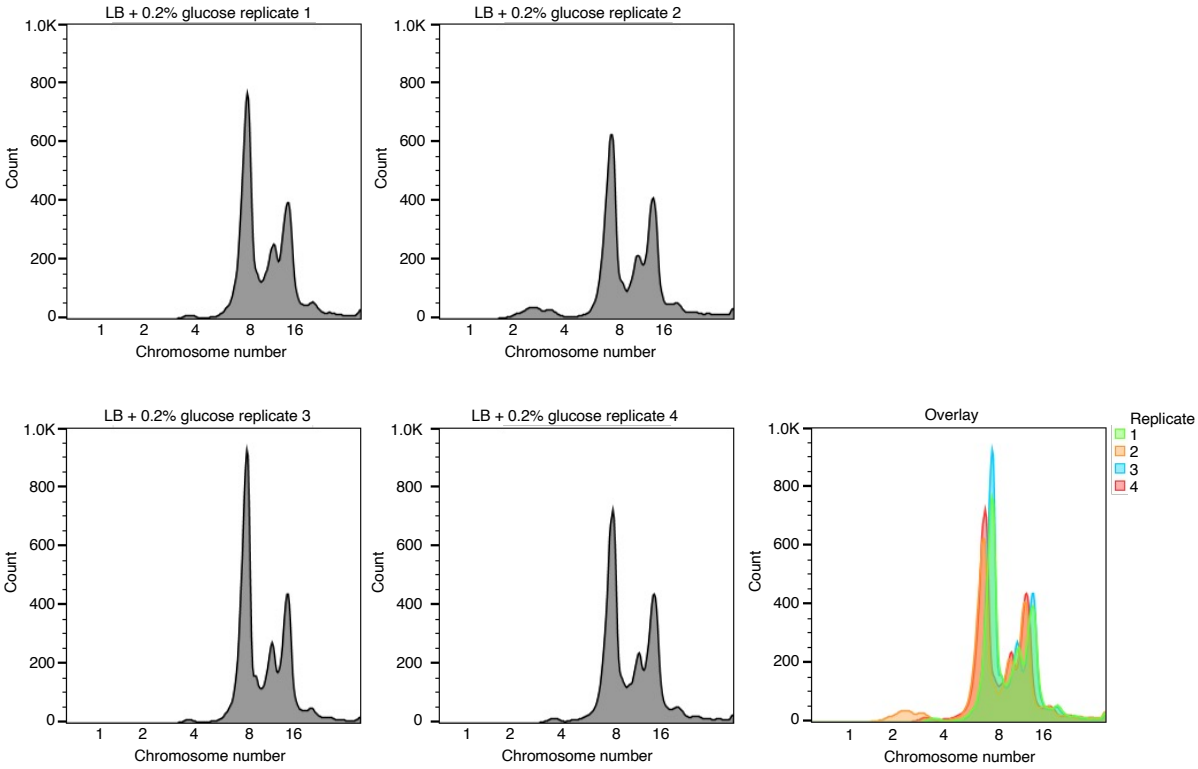

Figure S10 - Reproducibility of replication run-out assays for the Δ*bamB* strain
Flow cytometry of *E. coli* LCE-18 Δ*bamB* cells grown in LB supplemented with 0.2% glucose at 37°C with aeration before being treated with rifampicin, cephalexin and stained with Sytox Green. Fluorescence is plotted and represents chromosomal content for each cell with chromosome numbers for each peak marked. Each experiment was repeated on 4 separate occasions and an overlay of the separate data panels is presented.

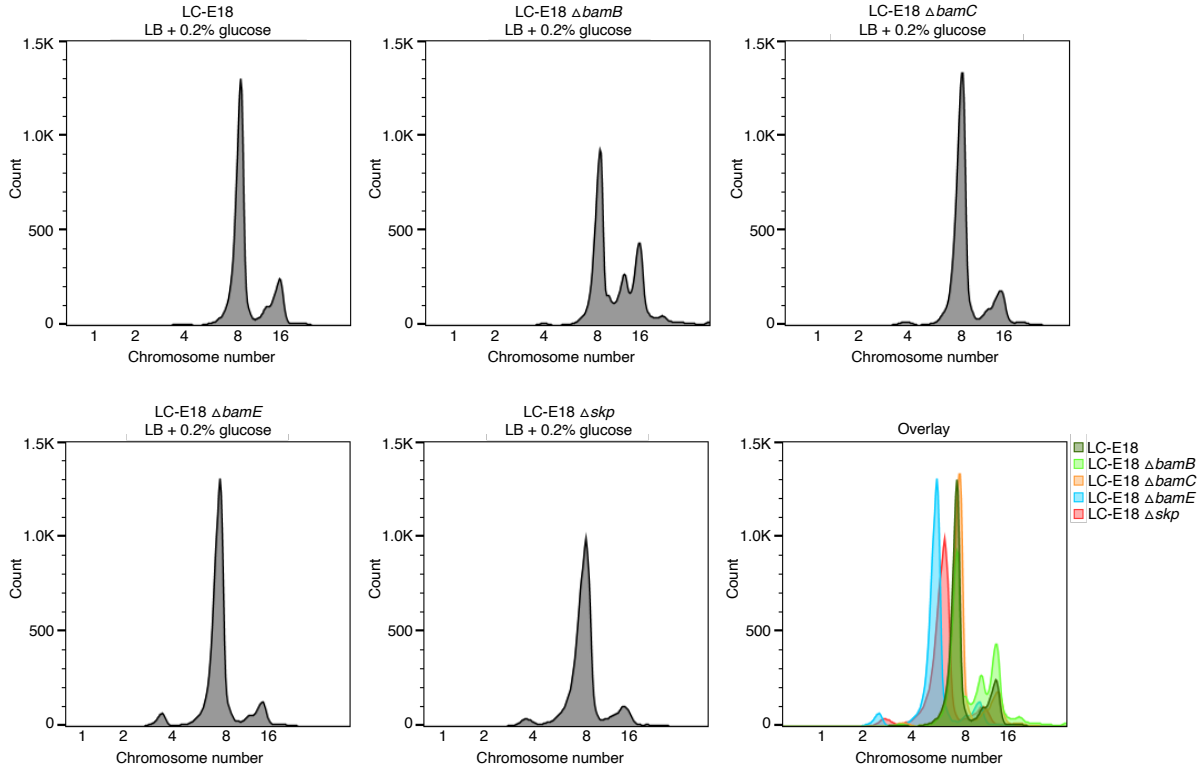

Figure S11 – Replication run-out assays for the parent, Δ*bamB*, Δ*bamC*, Δ*bamE* and Δ*skp* strains

Flow cytometry of *E. coli* LCE-18 WT parent, Δ*bamB*, Δ*bamC*, Δ*bamE* or Δ*skp* cells grown in LB supplemented with 0.2% glucose at 37°C with aeration before being treated with rifampicin, cephalexin and stained with Sytox Green. Fluorescence is plotted and represents chromosomal content for each cell with chromosome numbers for each peak marked. An overlay of the separate data panels is presented.

827 **Materials and methods**

828 **Bacterial strains and culture conditions.**

829 For TraDIS experiments, the parent strain was *E. coli* K-12 BW25113. The *E. coli* Δ*bamB*,
830 Δ*bamC*, Δ*bamE*, Δ*surA*, Δ*skp* and Δ*degP* mutants were generated by transferring the relevant
831 allele from the Keio library (Baba et al., 2006) into the clean parent strain by P1 transduction
832 (Thomason et al., 2007). The *kan*^{R} cassette was then removed by using the pCP20 plasmid
833 (Cherepanov & Wackernagel, 1995). These strains were then used for construction of
834 transposon libraries. The same approach was used for construction of the *E. coli* Δ*wecA*::*aph*,
835 Δ*wecD*::*aph*, Δ*wecF*::*aph*, Δ*ompT::aph,* Δ*dapF*::*aph* and Δ*diaA::aph* mutants. The *diaA::aph*
836 allele was also transferred into the Δ*bamB* derivative of *E. coli* BW25113 to generate the
837 Δ*bamB*Δ*diaA::aph* double mutant. The *dapF::aph* allele was also transferred from the Keio
838 library into Δ*bamB*, Δ*bamC*, Δ*bamE*, Δ*surA*, Δ*skp* and Δ*degP* mutants in the presence of 1
839 mM *meso*-diaminopimelate in order to generate double mutants. The Δ*rcsF*Δ*lpp*Δ*pgsA*Δ*surA*
840 mutant was generated by transfer of alleles from the Keio library and subsequent removal of
841 the *kan*^{R} cassette by use of the pCP20 plasmid before incorporation of the next allele by P1
842 transduction. The *E. coli* Δ*gmhA*::*aph,* Δ*gmhB*::*aph,* Δ*hldE*::*aph,* Δ*waaD*::*aph,* Δ*waaC*::*aph,*
843 Δ*waaF::aph,* Δ*waaP::aph,* Δ*waaG::aph,* Δ*waaY::aph* mutants were created by using λ-Red
844 recombination, as previously described for single-step gene inactivation (Datsenko & Wanner,
845 2000). All mutants were confirmed by polymerase chain reaction and strains were routinely
846 cultured on LB agar and LB broth. The dCas9 expressing strain *E. coli* LC-E18 and the
847 pSGRNA plasmid was a gift from David Bikard (Addgene plasmid # 115924) and has been
848 described previously (Cui et al., 2018). All strains used in this study are listed in **Table S3**.
849 Bacterial cultures were grown at 37°C unless otherwise stated. Where stated, the medium
850 was supplemented with kanamycin (50 µg/ml), carbenicillin (100 µg/ml), and *meso*-DAP (1
851 mM). For micro-dilution survival assays, bacteria were grown in 5 ml LB medium at 37°C with
852 aeration for ~16 hours. Cultures were normalised by optical density to OD_{600} = 1.00, 10-fold
853 serially diluted in LB, and 2 µl of each dilution was inoculated onto LB agar plates.

854

855 **Phenotypic screening**

856 The *E. coli* K-12 BW25113 parent strain, Δ*bamB*, Δ*bamC*, Δ*bamE*, Δ*surA*, Δ*skp* and Δ*degP*
857 mutants were screened against diverse stress conditions to phenotypically profile the mutants.
858 Strains were arrayed in 384-well format and inoculated on 2% agar LB plates using a BM3-
859 BC robot (S&P Robotic Inc.). In addition, the mutants and the wild type were subsequently
860 inoculated on LB agar plates containing different stress conditions. The inoculated plates were
861 incubated for 12 to 14 hours at 37°C before being imaged under controlled lighting with an 18-
862 megapixel Canon rebelT3i (Canon) camera on the BM3-BC robot (S&P Robotic Inc.). Images
863 of the plates were analysed using the software IRIS, which measured the size, opacity and
864 circularity of each colony (Kritikos et al., 2017). A total of 4 replica plates were generated for
865 each stress condition. Fitness of the mutants was then scored and analysed using the
866 ChemGAPP Small software (Doherty et al., 2023). Mean colony size for the mutant in each
867 condition was compared to the mean colony size of that mutant in the LB agar condition, which
868 was normalised to a fitness score of 1 (Doherty et al., 2023). Fitness scores below 1 represent
869 decreased fitness, as a function of colony size compared to growth on LB agar, and scores
870 above 1 indicate increased fitness in that condition. Each of the plates contained 56 replicates
871 for the parent BW25113 strain (WT), Δ*bamB*, Δ*bamC*, Δ*bamE* and Δ*degP* strains with 52
872 replicates for Δ*surA* and Δ*skp* for plate space requirements. There were 4 replicate plates for
873 each condition, all of which were treated as individual replicates and compared to their
874 respective wild type parent replicates on each plate before the average was taken. The
875 probability that the two means are equal across replicates was obtained by a one-way ANOVA.
876 Correlation of fitness ratios for each strain was assessed by calculating the Pearson
877 correlation coefficient for averaged fitness scores across replicates using Python before being
878 plotted as a heatmap.

879

880 **TraDIS library construction**

881 The *E. coli* K-12 BW25113 parent strain, Δ*bamB*, Δ*bamC*, Δ*bamE*, Δ*surA*, Δ*skp* and Δ*degP*
882 mutants were transformed with the EZ-Tn5™ <KAN-2> Tnp Transposome (Cambio) as
883 previously described (Goodall et al., 2021). Approximately 1 million mutant colonies were
884 pooled, thoroughly mixed and stored in LB supplemented with 15% glycerol at -80°C. DNA
885 was extracted from at least two samples of each transposon library to generate independent
886 sampling replicates for library generation.
887
888 **Sequencing of TraDIS libraries**
889 Cells from the pooled mutant library were harvested and genomic DNA was extracted for
890 library preparation and sequencing as previously described (Goodall et al., 2021). Samples
891 were sequenced using an Illumina MiSeq with a 150 cycle v3 cartridge.
892
893 **TraDIS data analysis**
894 Raw data were processed using a series of custom scripts as previously described (Goodall
895 et al., 2021). The data were trimmed using Fastx barcode splitter and trimmer tools (Pearson
896 *et al.,* 1997) and filtered based on inline indexes. The accuracy of the transposon sequences
897 were checked in two steps: the first 22 bases, allowing for three nucleotide base mismatches
898 and the last 10 bases of the transposon, allowing for up to one mismatch. Using Trimmomatic,
899 sequences with less than 20 bases in length were removed (Bolger *et al.,* 2014). TraDIS data
900 were then analysed using BioTraDIS (https://sanger-pathogens.github.io/Bio-Tradis/)
901 (Barquist et al., 2016) and aligned to the *E. coli* BW25113 reference genome CP009273.1,
902 available from NCBI (Tatusova *et al.,* 2014). We used SMALT
903 (https://www.sanger.ac.uk/tool/smalt/) as an aligner with zero value for mismatch threshold.
904 We also set the parameter smalt_r, determining how to treat multi-mapping reads, to zero.
905 This avoided repetitive elements to count as essential. We used the scripts
906 *tradis_essentiality.R and tradis_comparison.R* as part of the package to produce the list of
907 essentiality and then to compare the control and test libraries, respectively.
908

909 **Membrane fluidity assay**

910 Membrane fluidity was measured using the membrane fluidity kit (Abcam: ab189819), as
911 previously described, but with minor modifications (Bryant et al., 2020). Bacterial strains were
912 grown to mid-exponential phase (OD_{600} = ~0.4-0.6) in LB medium. Cells were harvested by
913 centrifugation, washed with phosphate buffered saline (PBS) and incubated with labelling mix
914 (10 μM pyrenedecanoic acid (PDA), 0.08% pluronic F-127, in PBS) in the dark for 20 min at
915 25°C with rocking. Cells were then washed twice in PBS and re-suspended in PBS prior to
916 measuring fluorescence (excitation = 350 nm, emission = either 400 nm or 470 nm).
917 Membrane fluidity was estimated by measuring the ratio of excimer (470 nm) to monomer (400
918 nm) fluorescence. The emission spectra were compared to unlabelled cells to confirm
919 membrane incorporation and each experiment contained triplicate technical repeats and was
920 then repeated three times. Membrane fluidity of the mutants of interest were expressed
921 relative to the parent *E. coli* strain. Experiments were performed in technical triplicate and
922 were repeated three times. Two sample t-tests were used to assess statistical significance of
923 differences from the WT strain.

924

925 **OmpT *in vivo* fluorescence assay**

926 The OmpT assay for monitoring Bam activity was performed as described previously with
927 minor modifications (Hagan et al., 2010, Iadanza et al., 2016, Storek et al., 2019). Bacterial
928 strains were grown to mid-exponential phase (OD_{600} = ~0.4-0.6) in LB medium and were
929 normalised to OD_{600} of 0.2 in growth media. The cell suspension (5 μl) was then added to 95
930 μl of 25 μM fluorogenic peptide, Abz-ARRAY(NO_2)-NH_2, diluted in PBS. Fluorescence
931 emission was immediately measured (excitation = 325 nm, emission = 430 nm) over a period
932 of 5 h, with readings every 20 s. OmpT activity was expressed relative to the parent strain.
933 Experiments were performed in technical triplicate and were repeated three times. Two
934 sample t-tests were used to assess statistical significance of differences from the WT strain.

935

936 **Phospholipid extraction and thin layer chromatography**

937 Phospholipids were extracted using an adapted Bligh-Dyer method (Bligh & Dyer, 1959).
938 Bacterial cultures were grown overnight (~16 hours) at 37°C with shaking and cells were
939 harvested by centrifugation. The bacterial cell pellets were resuspended and normalised to
940 OD_{600} = 3 and mixed with methanol and chloroform (2:1). The cell suspension was incubated
941 at 50°C for 30 min before additional chloroform and water was added to the samples to
942 produce a final ratio 2:2:1.8 of methanol/chloroform/water. Following centrifugation, the
943 phospholipid-containing phase was extracted and dried under nitrogen before being stored at
944 -20˚C. Samples were re-dissolved in chloroform before being separated by thin layer
945 chromatography on silica gel membrane using a solvent system that consisted of chloroform,
946 methanol, acetic acid (65:25:10). The plate was subsequently stained with phosphomolybdic
947 acid (PMA) and warmed until the lipid species were visible.
948
949 **Efficiency of plating assay**
950 Efficiency of plating assays were completed as previously described (Boelter et al., 2022).
951 Cells were grown overnight in LB (supplemented with 1 mM *meso*DAP where indicated) before
952 being normalised to OD_{600} = 1.00 and serially diluted 1:10. Following dilution, 2 μl was spotted
953 on agar plates containing supplements where indicated and incubated at 37°C for ~16 hours
954 before being imaged.
955
956 **Genetic interaction analysis**
957 For genetic interaction analysis, overnight cultures were diluted 1/100 and then grown to OD_{600}
958 = 0.8-1. Cultures were then spread on LB agar plates using sterile glass beads to create
959 source plates, before being incubated for 12 to 14 hours at 37˚C. Each strain was arrayed on
960 LB agar plates, from the source plates, to form 384 colonies of 96 replicates for each strain
961 using a BM3-BC robot (S&P Robotic Inc.). Plates were incubated at 37˚C for 12 to 14 hours.
962 The plate was then imaged under controlled lighting, with an 18-megapixel Canon rebelT3i
963 (Canon) camera on the BM3-BC robot (S&P Robotic Inc.). Images were then analysed using

964 the software called IRIS to measure the size, opacity and circularity of each colony on the
965 plates (Kritikos et al., 2017). Fitness of the mutants was then analysed and compared using
966 the software ChemGAPP GI (Doherty et al., 2023).
967
968 **Flow cytometry analysis**

969 Chromosome number measurements were performed as described previously, but with
970 several modifications (Hawkins et al., 2016). Briefly, cells were grown with aeration at 37°C
971 until OD_{600}=0.15 in LB medium supplemented with 0.2% glucose. Samples were collected,
972 treated with 150 µg/ml rifampicin, and 10 µg/ml cephalexin and incubated for 4 h at 37°C with
973 mixing. Incubation with antibiotics results in cells containing an integral number of
974 chromosomes, corresponding to the number of replication origins at the time of drug treatment.
975 Subsequently, cells were harvested, washed with TBS (20 mM Tris-HCl pH 7.5, 130 mM NaCl)
976 and fixed with cold 70% ethanol overnight. Additional samples were collected at OD_{600}=0.15
977 without antibiotic treatment and fixed as above.
978 Prior to flow cytometry analysis, cells were resuspended in 50 mM sodium citrate followed by
979 RNA digestion with RNase A for 4 h. Chromosomal DNA was stained with 2 mM Sytox Green
980 (Invitrogen) and DNA content per cell was measured with BD FACS Calibur at 488 nm Argon
981 Ion laser. MG1655 (WT) strain grown in AB medium containing one of the following carbon
982 sources: 0.4% sodium acetate, 0.2% glucose, 0.2% glucose + 0.5% casamino acids or in LB
983 medium with 0.2% glucose, treated with antibiotics, fixed and stained as above was used as
984 a standard for each flow cytometry measurement, indicating cells containing 1/2 , 2/4, 4/8 or
985 8/16 chromosomes, respectively. Flow cytometry data was analyzed using FlowJo ver. 10.8.0.
986
987 **Conservation analysis**

988 Reference genomes were downloaded for each species from NCBI in fasta format and
989 annotated using Prokka (Seemann, 2014). The 16s rRNA sequence for each species was
990 then extracted from Prokka ffn files in fasta format. A Kmer based neighbour joining tree was

991 produced via extracting a one-step sliding window of 8 base kmers from each 16s rRNA
992 sequence. Following this, the number of unique kmers was counted for each species in order
993 to produce a Kmer profile. The Jaccard similarity between each species Kmer profiles was
994 then used to produce a distance matrix. This distance matrix was input into the R module
995 ape::nj to produce the neighbour joining tree. The neighbour joining tree was reformatted as
996 a nexus file and visualised within Figtree (http://tree.bio.ed.ac.uk/software/figtree/), where the
997 tree was rooted at the midpoint and branches were transformed to become proportional.
998 To count the instances of the proteins BamA, BamB, BamC, BamD, BamE, DegP, SurA, and
999 Skp, hmmsearch was used to extract proteins with the relevant domains from the Prokka
1000 annotated faa files. The Pfam domains used were PF01103, PF13360, PF06804, PF13525,
1001 PF04355, PF09312 and PF03938 for BamA, BamB, BamC, BamD, BamE, SurA, and Skp,
1002 respectively. For DegP, both PF00595 and PF13180 were used and the intersect taken. An
1003 e-value of 0.001 was used as a threshold for significant hits by hmmsearch. For BamA, hits
1004 annotated as the query protein were inputted into hmmscan and hits with at least one POTRA
1005 domain and an Omp85 domain were counted as true BamA hits. Hits containing a Tam-
1006 POTRA domain were excluded. Where a hit had only an Omp85 gene, the adjacent gene was
1007 checked for the POTRA domains. For BamB, any hmmsearch hits annotated as BamB or
1008 hypothetical proteins by Prokka were input into SignalP 6.0 (Teufel et al., 2022) and hmmscan.
1009 Proteins assigned a LIPO (Sec/SPII) signal peptide within SignalP 6.0, with only one PQQ_2
1010 domain within hmmscan were selected as true BamB hits. For BamC, all hits from hmmsearch
1011 were inputted into hmmscan to confirm the presence of the Lipoprotein-18 domain. Hits were
1012 also inputted into Phmmer and proteins with significant homology to BamC were counted as
1013 true hits. For BamD, hypothetical proteins and BamD hits were inputted into hmmscan and
1014 Phmmer and those with homology to BamD and a non-outcompeted YfiO domain counted as
1015 true hits. For BamE, hypothetical proteins and BamE hits were inputted into hmmscan and
1016 those with a singular SmpA_OmlA domain were counted as true hits. For DegP hypothetical
1017 proteins and DegP hits were inputted into hmmscan. If a hit had a PDZ type domain,
1018 Peptidase_M50 domain or Trypsin_2 domain then it was visualised on Pfam and manually

1019 assigned as DegP based on structure. If a DegP hit had any other type of domain, it was
1020 discounted. For SurA, all hits were run through hmmscan and Phmmer. Those with a SurA_N
1021 domain, Rotamase domain and a Rotamase_3 domain and homologous to SurA within
1022 Phmmer were counted. For Skp, all hits were run through Phmmer and only hits with only an
1023 OmpH domain and with homology to Skp counted as true hits. Finally, the neighbour-joining
1024 tree was edited in iTOL (Letunic & Bork, 2021) to produce the heatmap of gene counts.
1025

1026 **References**

1027

1028 Baba T, Ara T, Hasegawa M, Takai Y, Okumura Y, Baba M, Datsenko KA, Tomita M, Wanner BL,
1029 Mori H (2006) Construction of Escherichia coli K-12 in-frame, single-gene knockout mutants:
1030 the Keio collection. Mol Syst Biol 2: 2006.0008
1031 Bakelar J, Buchanan SK, Noinaj N (2016) The structure of the beta-barrel assembly machinery
1032 complex. Science 351: 180-6
1033 Barquist L, Mayho M, Cummins C, Cain AK, Boinett CJ, Page AJ, Langridge GC, Quail MA, Keane
1034 JA, Parkhill J (2016) The TraDIS toolkit: sequencing and analysis for dense transposon mutant
1035 libraries. Bioinformatics 32: 1109-11
1036 Bligh EG, Dyer WJ (1959) A rapid method of total lipid extraction and purification. Can J
1037 Biochem Physiol 37: 911-7
1038 Boelter G, Bryant JA, Doherty H, Wotherspoon P, Alodaini D, Ma X, Alao MB, Moynihan PJ,
1039 Moradigaravand D, Glinkowska M, Knowles TJ, Henderson IR, Banzhaf M (2022) The lipoprotein
1040 DolP affects cell separation in Escherichia coli, but not as an upstream regulator of NlpD.
1041 Microbiology (Reading) 168
1042 Browning DF, Bavro VN, Mason JL, Sevastsyanovich YR, Rossiter AE, Jeeves M, Wells TJ, Knowles
1043 TJ, Cunningham AF, Donald JW, Palmer T, Overduin M, Henderson IR (2015) Cross-species
1044 chimeras reveal BamA POTRA and β-barrel domains must be fine-tuned for efficient OMP
1045 insertion. Mol Microbiol 97: 646-59
1046 Bryant JA, Morris FC, Knowles TJ, Maderbocus R, Heinz E, Boelter G, Alodaini D, Colyer A,
1047 Wotherspoon PJ, Staunton KA, Jeeves M, Browning DF, Sevastsyanovich YR, Wells TJ, Rossiter
1048 AE, Bavro VN, Sridhar P, Ward DG, Chong ZS, Goodall EC et al. (2020) Structure of dual BON-
1049 domain protein DolP identifies phospholipid binding as a new mechanism for protein
1050 localisation. Elife 9
1051 Cain AK, Barquist L, Goodman AL, Paulsen IT, Parkhill J, van Opijnen T (2020) A decade of
1052 advances in transposon-insertion sequencing. Nat Rev Genet 21: 526-540
1053 Camara JE, Breier AM, Brendler T, Austin S, Cozzarelli NR, Crooke E (2005) Hda inactivation of
1054 DnaA is the predominant mechanism preventing hyperinitiation of Escherichia coli DNA
1055 replication. EMBO Rep 6: 736-41
1056 Camara JE, Skarstad K, Crooke E (2003) Controlled initiation of chromosomal replication in
1057 Escherichia coli requires functional Hda protein. J Bacteriol 185: 3244-8
1058 Castanié-Cornet MP, Cam K, Jacq A (2006) RcsF is an outer membrane lipoprotein involved in
1059 the RcsCDB phosphorelay signaling pathway in Escherichia coli. J Bacteriol 188: 4264-70
1060 Charlson ES, Werner JN, Misra R (2006) Differential effects of yfgL mutation on Escherichia coli
1061 outer membrane proteins and lipopolysaccharide. J Bacteriol 188: 7186-94
1062 Cherepanov PP, Wackernagel W (1995) Gene disruption in Escherichia coli: TcR and KmR
1063 cassettes with the option of Flp-catalyzed excision of the antibiotic-resistance determinant.
1064 Gene 158: 9-14
1065 Cooper DL, Harada T, Tamazi S, Ferrazzoli AE, Lovett ST (2021) The Role of Replication Clamp-
1066 Loader Protein HolC of Escherichia coli in Overcoming Replication/Transcription Conflicts. mBio
1067 12
1068 Cooper S, Helmstetter CE (1968) Chromosome replication and the division cycle of Escherichia
1069 coli B/r. J Mol Biol 31: 519-540
1070 Cui L, Vigouroux A, Rousset F, Varet H, Khanna V, Bikard D (2018) A CRISPRi screen in E. coli
1071 reveals sequence-specific toxicity of dCas9. Nat Commun 9: 1912

d'Alençon E, Taghbalout A, Kern R, Kohiyama M (1999) Replication cycle dependent association of SeqA to the outer membrane fraction of E. coli. Biochimie 81: 841-6

Danese PN, Oliver GR, Barr K, Bowman GD, Rick PD, Silhavy TJ (1998) Accumulation of the enterobacterial common antigen lipid II biosynthetic intermediate stimulates degP transcription in Escherichia coli. J Bacteriol 180: 5875-84

Datsenko KA, Wanner BL (2000) One-step inactivation of chromosomal genes in Escherichia coli K-12 using PCR products. Proc Natl Acad Sci U S A 97: 6640-5

Davies BW, Kohanski MA, Simmons LA, Winkler JA, Collins JJ, Walker GC (2009) Hydroxyurea induces hydroxyl radical-mediated cell death in Escherichia coli. Mol Cell 36: 845-60

Dewey DL, Work E (1952) Diaminopimelic acid decarboxylase. Nature 169: 533-4

Doherty HM, Kritikos G, Galardini M, Banzhaf M, Moradigaravand D (2023) ChemGAPP: a tool for chemical genomics analysis and phenotypic profiling. Bioinformatics 39

Dong C, Hou HF, Yang X, Shen YQ, Dong YH (2012) Structure of Escherichia coli BamD and its functional implications in outer membrane protein assembly. Acta Crystallogr D Biol Crystallogr 68: 95-101

Doyle MT, Jimah JR, Dowdy T, Ohlemacher SI, Larion M, Hinshaw JE, Bernstein HD (2022) Cryo-EM structures reveal multiple stages of bacterial outer membrane protein folding. Cell 185: 1143-1156.e13

Garner J, Durrer P, Kitchen J, Brunner J, Crooke E (1998) Membrane-mediated release of nucleotide from an initiator of chromosomal replication, Escherichia coli DnaA, occurs with insertion of a distinct region of the protein into the lipid bilayer. J Biol Chem 273: 5167-73

Gentle IE, Burri L, Lithgow T (2005) Molecular architecture and function of the Omp85 family of proteins. Mol Microbiol 58: 1216-25

Goodall ECA, Isom GL, Rooke JL, Pullela K, Icke C, Yang Z, Boelter G, Jones A, Warner I, Da Costa R, Zhang B, Rae J, Tan WB, Winkle M, Delhaye A, Heinz E, Collet JF, Cunningham AF, Blaskovich MA, Parton RG et al. (2021) Loss of YhcB results in dysregulation of coordinated peptidoglycan, LPS and phospholipid synthesis during Escherichia coli cell growth. PLoS Genet 17: e1009586

Gronow S, Brabetz W, Brade H (2000) Comparative functional characterization in vitro of heptosyltransferase I (WaaC) and II (WaaF) from Escherichia coli. Eur J Biochem 267: 6602-11

Gu Y, Li H, Dong H, Zeng Y, Zhang Z, Paterson NG, Stansfeld PJ, Wang Z, Zhang Y, Wang W, Dong C (2016) Structural basis of outer membrane protein insertion by the BAM complex. Nature 531: 64-9

Hagan CL, Kim S, Kahne D (2010) Reconstitution of outer membrane protein assembly from purified components. Science 328: 890-2

Harris LK, Theriot JA (2016) Relative Rates of Surface and Volume Synthesis Set Bacterial Cell Size. Cell 165: 1479-1492

Hart EM, Gupta M, Wühr M, Silhavy TJ (2019) The Synthetic Phenotype of ΔbamB ΔbamE Double Mutants Results from a Lethal Jamming of the Bam Complex by the Lipoprotein RcsF. mBio 10

Hart EM, Silhavy TJ (2020) Functions of the BamBCDE Lipoproteins Revealed by Bypass Mutations in BamA. J Bacteriol 202

Hawkins M, Atkinson J, McGlynn P (2016) Escherichia coli Chromosome Copy Number Measurement Using Flow Cytometry Analysis. Methods Mol Biol 1431: 151-9

Iadanza MG, Higgins AJ, Schiffrin B, Calabrese AN, Brockwell DJ, Ashcroft AE, Radford SE, Ranson NA (2016) Lateral opening in the intact beta-barrel assembly machinery captured by cryo-EM. Nat Commun 7: 12865

1118 Ishida T, Akimitsu N, Kashioka T, Hatano M, Kubota T, Ogata Y, Sekimizu K, Katayama T (2004)
1119 DiaA, a novel DnaA-binding protein, ensures the timely initiation of Escherichia coli
1120 chromosome replication. Journal of Biological Chemistry 279: 45546-45555
1121 Jameson KH, Wilkinson AJ (2017) Control of initiation of DNA replication in Bacillus subtilis and
1122 Escherichia coli. Genes 8: 22
1123 Jorgenson MA, Kannan S, Laubacher ME, Young KD (2016) Dead-end intermediates in the
1124 enterobacterial common antigen pathway induce morphological defects in Escherichia coli by
1125 competing for undecaprenyl phosphate. Mol Microbiol 100: 1-14
1126 Kadrmas JL, Raetz CR (1998) Enzymatic synthesis of lipopolysaccharide in Escherichia coli.
1127 Purification and properties of heptosyltransferase i. J Biol Chem 273: 2799-807
1128 Kajimura J, Rahman A, Rick PD (2005) Assembly of cyclic enterobacterial common antigen in
1129 Escherichia coli K-12. J Bacteriol 187: 6917-27
1130 Katayama T, Kubota T, Kurokawa K, Crooke E, Sekimizu K (1998) The initiator function of DnaA
1131 protein is negatively regulated by the sliding clamp of the E. coli chromosomal replicase. Cell
1132 94: 61-71
1133 Kato J, Katayama T (2001) Hda, a novel DnaA-related protein, regulates the replication cycle in
1134 Escherichia coli. Embo j 20: 4253-62
1135 Keyamura K, Fujikawa N, Ishida T, Ozaki S, Su'etsugu M, Fujimitsu K, Kagawa W, Yokoyama S,
1136 Kurumizaka H, Katayama T (2007) The interaction of DiaA and DnaA regulates the replication
1137 cycle in E. coli by directly promoting ATP–DnaA-specific initiation complexes. Genes &
1138 development 21: 2083-2099
1139 Kikuchi S, Shibuya I, Matsumoto K (2000) Viability of an Escherichia coli pgsA null mutant
1140 lacking detectable phosphatidylglycerol and cardiolipin. J Bacteriol 182: 371-6
1141 Kneidinger B, Marolda C, Graninger M, Zamyatina A, McArthur F, Kosma P, Valvano MA,
1142 Messner P (2002) Biosynthesis pathway of ADP-l-glycero-β-d-manno-heptose in Escherichia
1143 coli. J Bacteriol 184: 363-369
1144 Knowles TJ, Browning DF, Jeeves M, Maderbocus R, Rajesh S, Sridhar P, Manoli E, Emery D,
1145 Sommer U, Spencer A, Leyton DL, Squire D, Chaudhuri RR, Viant MR, Cunningham AF,
1146 Henderson IR, Overduin M (2011) Structure and function of BamE within the outer membrane
1147 and the beta-barrel assembly machine. EMBO Rep 12: 123-8
1148 Knowles TJ, Jeeves M, Bobat S, Dancea F, McClelland D, Palmer T, Overduin M, Henderson IR
1149 (2008) Fold and function of polypeptide transport-associated domains responsible for
1150 delivering unfolded proteins to membranes. Mol Microbiol 68: 1216-27
1151 Konovalova A, Kahne DE, Silhavy TJ (2017) Outer Membrane Biogenesis. Annu Rev Microbiol
1152 71: 539-556
1153 Konovalova A, Mitchell AM, Silhavy TJ (2016) A lipoprotein/beta-barrel complex monitors
1154 lipopolysaccharide integrity transducing information across the outer membrane. Elife 5
1155 Kritikos G, Banzhaf M, Herrera-Dominguez L, Koumoutsi A, Wartel M, Zietek M, Typas A (2017)
1156 A tool named Iris for versatile high-throughput phenotyping in microorganisms. Nature
1157 microbiology 2: 17014
1158 Krojer T, Sawa J, Schäfer E, Saibil HR, Ehrmann M, Clausen T (2008) Structural basis for the
1159 regulated protease and chaperone function of DegP. Nature 453: 885-90
1160 Kuhn HM, Meier-Dieter U, Mayer H (1988) ECA, the enterobacterial common antigen. FEMS
1161 Microbiol Rev 4: 195-222
1162 Kuhn HM, Neter E, Mayer H (1983) Modification of the lipid moiety of the enterobacterial
1163 common antigen by the "Pseudomonas factor". Infection and immunity 40: 696-700

1164 Kumar GS, Jagannadham MV, Ray MK (2002) Low-temperature-induced changes in
1165 composition and fluidity of lipopolysaccharides in the antarctic psychrotrophic bacterium
1166 Pseudomonas syringae. J Bacteriol 184: 6746-9
1167 Kunin CM (1963) SEPARATION, CHARACTERIZATION, AND BIOLOGICAL SIGNIFICANCE OF A
1168 COMMON ANTIGEN IN ENTEROBACTERIACEAE. J Exp Med 118: 565-86
1169 Langridge GC, Phan MD, Turner DJ, Perkins TT, Parts L, Haase J, Charles I, Maskell DJ, Peters SE,
1170 Dougan G, Wain J, Parkhill J, Turner AK (2009) Simultaneous assay of every Salmonella Typhi
1171 gene using one million transposon mutants. Genome Res 19: 2308-16
1172 Lazar SW, Kolter R (1996) SurA assists the folding of Escherichia coli outer membrane proteins.
1173 J Bacteriol 178: 1770-3
1174 Letunic I, Bork P (2021) Interactive Tree Of Life (iTOL) v5: an online tool for phylogenetic tree
1175 display and annotation. Nucleic Acids Res 49: W293-w296
1176 Li G, He C, Bu P, Bi H, Pan S, Sun R, Zhao XS (2018) Single-Molecule Detection Reveals Different
1177 Roles of Skp and SurA as Chaperones. ACS Chem Biol 13: 1082-1089
1178 Lu M, Campbell JL, Boye E, Kleckner N (1994) SeqA: a negative modulator of replication
1179 initiation in E. coli. Cell 77: 413-26
1180 Malinverni JC, Silhavy TJ (2011) Assembly of Outer Membrane β-Barrel Proteins: the Bam
1181 Complex. EcoSal Plus 4
1182 Mamou G, Corona F, Cohen-Khait R, Housden NG, Yeung V, Sun D, Sridhar P, Pazos M, Knowles
1183 TJ, Kleanthous C, Vollmer W (2022) Peptidoglycan maturation controls outer membrane
1184 protein assembly. Nature 606: 953-959
1185 Marolda CL, Valvano MA (1995) Genetic analysis of the dTDP-rhamnose biosynthesis region of
1186 the Escherichia coli VW187 (O7:K1) rfb gene cluster: identification of functional homologs of
1187 rfbB and rfbA in the rff cluster and correct location of the rffE gene. J Bacteriol 177: 5539-46
1188 Mengin-Lecreulx D, Michaud C, Richaud C, Blanot D, van Heijenoort J (1988) Incorporation of
1189 LL-diaminopimelic acid into peptidoglycan of Escherichia coli mutants lacking diaminopimelate
1190 epimerase encoded by dapF. J Bacteriol 170: 2031-9
1191 Mickiewicz KM, Kawai Y, Drage L, Gomes MC, Davison F, Pickard R, Hall J, Mostowy S, Aldridge
1192 PD, Errington J (2019) Possible role of L-form switching in recurrent urinary tract infection. Nat
1193 Commun 10: 4379
1194 Mitchell AM, Srikumar T, Silhavy TJ (2018) Cyclic Enterobacterial Common Antigen Maintains
1195 the Outer Membrane Permeability Barrier of Escherichia coli in a Manner Controlled by YhdP.
1196 mBio 9
1197 Morris KN, Mitchell AM (2023) Phosphatidylglycerol Is the Lipid Donor for Synthesis of
1198 Phospholipid-Linked Enterobacterial Common Antigen. J Bacteriol: e0040322
1199 Nakayashiki T, Mori H (2013) Genome-wide screening with hydroxyurea reveals a link between
1200 nonessential ribosomal proteins and reactive oxygen species production. J Bacteriol 195: 1226-
1201 35
1202 Nichols RJ, Sen S, Choo YJ, Beltrao P, Zietek M, Chaba R, Lee S, Kazmierczak KM, Lee KJ, Wong
1203 A, Shales M, Lovett S, Winkler ME, Krogan NJ, Typas A, Gross CA (2011) Phenotypic landscape
1204 of a bacterial cell. Cell 144: 143-56
1205 Parker CT, Kloser AW, Schnaitman CA, Stein MA, Gottesman S, Gibson BW (1992) Role of the
1206 rfaG and rfaP genes in determining the lipopolysaccharide core structure and cell surface
1207 properties of Escherichia coli K-12. J Bacteriol 174: 2525-38
1208 Rai AK, Carr JF, Bautista DE, Wang W, Mitchell AM (2021) ElyC and Cyclic Enterobacterial
1209 Common Antigen Regulate Synthesis of Phosphoglyceride-Linked Enterobacterial Common
1210 Antigen. mBio 12: e0284621

1211 Rai AK, Mitchell AM (2020) Enterobacterial Common Antigen: Synthesis and Function of an
1212 Enigmatic Molecule. mBio 11
1213 Ranava D, Yang Y, Orenday-Tapia L, Rousset F, Turlan C, Morales V, Cui L, Moulin C, Froment C,
1214 Munoz G, Rech J, Marcoux J, Caumont-Sarcos A, Albenne C, Bikard D, Ieva R (2021) Lipoprotein
1215 DolP supports proper folding of BamA in the bacterial outer membrane promoting fitness upon
1216 envelope stress. Elife 10
1217 Richaud C, Higgins W, Mengin-Lecreulx D, Stragier P (1987) Molecular cloning,
1218 characterization, and chromosomal localization of dapF, the Escherichia coli gene for
1219 diaminopimelate epimerase. J Bacteriol 169: 1454-9
1220 Rizzitello AE, Harper JR, Silhavy TJ (2001) Genetic evidence for parallel pathways of chaperone
1221 activity in the periplasm of Escherichia coli. J Bacteriol 183: 6794-800
1222 Rojas ER, Billings G, Odermatt PD, Auer GK, Zhu L, Miguel A, Chang F, Weibel DB, Theriot JA,
1223 Huang KC (2018) The outer membrane is an essential load-bearing element in Gram-negative
1224 bacteria. Nature 559: 617-621
1225 Rollauer SE, Sooreshjani MA, Noinaj N, Buchanan SK (2015) Outer membrane protein
1226 biogenesis in Gram-negative bacteria. Philos Trans R Soc Lond B Biol Sci 370
1227 Rotman E, Bratcher P, Kuzminov A (2009) Reduced lipopolysaccharide phosphorylation in
1228 Escherichia coli lowers the elevated ori/ter ratio in seqA mutants. Mol Microbiol 72: 1273-92
1229 Rouvière PE, Gross CA (1996) SurA, a periplasmic protein with peptidyl-prolyl isomerase
1230 activity, participates in the assembly of outer membrane porins. Genes Dev 10: 3170-82
1231 Rowlett VW, Mallampalli V, Karlstaedt A, Dowhan W, Taegtmeyer H, Margolin W, Vitrac H
1232 (2017) Impact of Membrane Phospholipid Alterations in Escherichia coli on Cellular Function
1233 and Bacterial Stress Adaptation. J Bacteriol 199
1234 Ruiz N, Kahne D, Silhavy TJ (2006) Advances in understanding bacterial outer-membrane
1235 biogenesis. Nat Rev Microbiol 4: 57-66
1236 Sánchez-Pulido L, Devos D, Genevrois S, Vicente M, Valencia A (2003) POTRA: a conserved
1237 domain in the FtsQ family and a class of beta-barrel outer membrane proteins. Trends in
1238 biochemical sciences 28: 523-6
1239 Sandoval CM, Baker SL, Jansen K, Metzner SI, Sousa MC (2011) Crystal structure of BamD: an
1240 essential component of the β-Barrel assembly machinery of gram-negative bacteria. J Mol Biol
1241 409: 348-57
1242 Schmidt G, Mannel D, Mayer H, Whang HY, Neter E (1976) Role of a lipopolysaccharide gene
1243 for immunogenicity of the enterobacterial common antigen. J Bacteriol 126: 579-86
1244 Seemann T (2014) Prokka: rapid prokaryotic genome annotation. Bioinformatics 30: 2068-9
1245 Sekimizu K, Kornberg A (1988) Cardiolipin activation of dnaA protein, the initiation protein of
1246 replication in Escherichia coli. J Biol Chem 263: 7131-5
1247 Si F, Li D, Cox SE, Sauls JT, Azizi O, Sou C, Schwartz AB, Erickstad MJ, Jun Y, Li X, Jun S (2017)
1248 Invariance of Initiation Mass and Predictability of Cell Size in Escherichia coli. Curr Biol 27: 1278-
1249 1287
1250 Simpson BW, Trent MS (2019) Pushing the envelope: LPS modifications and their
1251 consequences. Nat Rev Microbiol 17: 403-416
1252 Sivaraman J, Sauvé V, Matte A, Cygler M (2002) Crystal structure of Escherichia coli glucose-1-
1253 phosphate thymidylyltransferase (RffH) complexed with dTTP and Mg2+. J Biol Chem 277:
1254 44214-9
1255 Sklar JG, Wu T, Kahne D, Silhavy TJ (2007) Defining the roles of the periplasmic chaperones
1256 SurA, Skp, and DegP in Escherichia coli. Genes Dev 21: 2473-84

Steenhuis M, van Ulsen P, Martin NI, Luirink J (2021) A ban on BAM: an update on inhibitors of the β-barrel assembly machinery. FEMS Microbiol Lett 368

Storek KM, Auerbach MR, Shi H, Garcia NK, Sun D, Nickerson NN, Vij R, Lin Z, Chiang N, Schneider K, Wecksler AT, Skippington E, Nakamura G, Seshasayee D, Koerber JT, Payandeh J, Smith PA, Rutherford ST (2018) Monoclonal antibody targeting the β-barrel assembly machine of Escherichia coli is bactericidal. Proc Natl Acad Sci U S A 115: 3692-3697

Storek KM, Vij R, Sun D, Smith PA, Koerber JT, Rutherford ST (2019) The Escherichia coli β-Barrel Assembly Machinery Is Sensitized to Perturbations under High Membrane Fluidity. J Bacteriol 201

Sutera VA, Jr., Lovett ST (2006) The role of replication initiation control in promoting survival of replication fork damage. Mol Microbiol 60: 229-39

Suzuki M, Hara H, Matsumoto K (2002) Envelope disorder of Escherichia coli cells lacking phosphatidylglycerol. J Bacteriol 184: 5418-25

Tata M, Konovalova A (2019) Improper Coordination of BamA and BamD Results in Bam Complex Jamming by a Lipoprotein Substrate. mBio 10

Teufel F, Almagro Armenteros JJ, Johansen AR, Gíslason MH, Pihl SI, Tsirigos KD, Winther O, Brunak S, von Heijne G, Nielsen H (2022) SignalP 6.0 predicts all five types of signal peptides using protein language models. Nat Biotechnol 40: 1023-1025

Thewasano N, Germany EM, Maruno Y, Nakajima Y, Shiota T Categorization of Escherichia coli Outer Membrane Proteins by Dependence on Accessory Proteins of the β-barrel Assembly Machinery Complex. Journal of Biological Chemistry

Thomason LC, Costantino N, Court DL (2007) E. coli genome manipulation by P1 transduction. Curr Protoc Mol Biol Chapter 1: 1.17.1-1.17.8

Tomasek D, Rawson S, Lee J, Wzorek JS, Harrison SC, Li Z, Kahne D (2020) Structure of a nascent membrane protein as it folds on the BAM complex. Nature 583: 473-478

Torheim NK, Skarstad K (1999) Escherichia coli SeqA protein affects DNA topology and inhibits open complex formation at oriC. Embo j 18: 4882-8

Valvano MA (2022) Remodelling of the Gram-negative bacterial Kdo(2)-lipid A and its functional implications. Microbiology (Reading) 168

von Freiesleben U, Rasmussen KV, Schaechter M (1994) SeqA limits DnaA activity in replication from oriC in Escherichia coli. Mol Microbiol 14: 763-772

Wallden M, Fange D, Lundius EG, Baltekin Ö, Elf J (2016) The Synchronization of Replication and Division Cycles in Individual E. coli Cells. Cell 166: 729-739

Webb CT, Chandrapala D, Oslan SN, Bamert RS, Grinter RD, Dunstan RA, Gorrell RJ, Song J, Strugnell RA, Lithgow T, Kwok T (2017) Reductive evolution in outer membrane protein biogenesis has not compromised cell surface complexity in Helicobacter pylori. Microbiologyopen 6

Webb CT, Heinz E, Lithgow T (2012) Evolution of the β-barrel assembly machinery. Trends in microbiology 20: 612-20

Winkle M, Hernández-Rocamora VM, Pullela K, Goodall ECA, Martorana AM, Gray J, Henderson IR, Polissi A, Vollmer W (2021) DpaA Detaches Braun's Lipoprotein from Peptidoglycan. mBio 12

Wu T, Malinverni J, Ruiz N, Kim S, Silhavy TJ, Kahne D (2005) Identification of a multicomponent complex required for outer membrane biogenesis in Escherichia coli. Cell 121: 235-45

Yethon JA, Heinrichs DE, Monteiro MA, Perry MB, Whitfield C (1998) Involvement of waaY, waaQ, and waaP in the modification of Escherichia coli lipopolysaccharide and their role in the formation of a stable outer membrane. J Biol Chem 273: 26310-6

1304